Optical and X-ray Study of the Low Plagioclases

by

Hugh E. Wolfe

Thesis submitted to the Graduate Faculty of the

Virginia Polytechnic Institute and State University

in partial fulfillment of the requirements for the degree of

MASTER OF SCIENCE

in

Geological Sciences

APPROVED:

F. D. Bloss

F. D. Bloss, Chairman

P. H. Ribbe

P. H. Ribbe

G. V. Gibbs

G. V. Gibbs

May, 1976

Blacksburg, Virginia

ACKNOWLEDGEMENTS

It is a pleasure to acknowledge the advice and encouragement extended to me by members of my advisory committee: Professors F. Donald Bloss, Paul H. Ribbe, and Gerald V. Gibbs.

TABLE OF CONTENTS

LIST OF TABLES

LIST OF FIGURES

INTRODUCTION

The spindle stage techniques of Bloss and Riess (1973), coupled with those more recently developed by Bloss and co-workers, make possible routine optical measurements of greater accuracy than have heretofore been possible. The techniques are such that the optic axial angle, 2V, can be measured to a fraction of a degree, the principal refractive indices for various wavelengths to within 0.0002, and the principal vibration axes X, Y, and Z can be located within a degree. Moreover, by using a Supper spindle stage, which accomodates an x-ray goniometer head, the directions of the unit cell vectors may be determined relative to the orientation of the optical indicatrix at various wavelengths. A major advantage of the spindle stage is that all these measurements plus a microprobe analysis may be made on a single grain. With so powerful a technique at hand it was decided to test it severely by applying it to the plagioclase feldspars (Table 1), a group whose optical properties have been studied by more workers than any other.

Table 1

Plagioclase Specimens

Specimen #	Reference #	Reference	Locality
1	99	Corlett and Eberhard (1967)	Amelia, Virginia USA
2	110	Corlett and Eberhard (1967)	Skarnbergbugten, Norway
3	129	Corlett and Eberhard (1967)	Gregory Bottly, Norway
4	294	Corlett and Eberhard (1967)	Camedo, Switzerland
5	170	Corlett and Eberhard (1967)	Kragero, Norway
6	31	Corlett and Eberhard (1967)	Quebec, Canada
7	7123	Speer and Ribbe (1973)	Kiglapait intrusion, Labrador
8	7106	Speer and Ribbe (1973)	Kiglapait intrusion, Labrador
9	33	Gay (1956)	Knoydort, Scotland
10	7122a	Speer and Ribbe (1973)	Kiglapait intrusion, Labrador
11	94	Corlett and Eberhard (1967)	Sannidal, Norway
12	7122b	Speer and Ribbe (1973)	Kiglapait intrusion, Labrador
13	7136	Speer and Ribbe (1973)	Kiglapait intrusion, Labrador
14	85	Corlett and Eberhard (1967)	Essex County, New York USA
15	22	Gay (1956)	Beaver Bay, Minnesota USA
16	7103	Speer and Ribbe (1973)	Kiglapait intrusion, Labrador
17	7131	Speer and Ribbe (1973)	Kiglapait intrusion, Labrador
18	7133	Speer and Ribbe (1973)	Kiglapait intrusion, Labrador
19	7111	Speer and Ribbe (1973)	Kiglapait intrusion, Labrador
20	7119	Speer and Ribbe (1973)	Kiglapait intrusion, Labrador
21	2043a	Speer and Ribbe (1973)	Kiglapait intrusion, Labrador
22	2043b	Speer and Ribbe (1973)	Kiglapait intrusion, Labrador
23	7100	Speer and Ribbe (1973)	Kiglapait intrusion, Labrador
24	7101	Speer and Ribbe (1973)	Kiglapait intrusion, Labrador
25	7113	Speer and Ribbe (1973)	Kiglapait intrusion, Labrador

Table 1 (con't)

26	4087	Gay and Muir (1963)	Skaergaard intrusion, Greenland
27	7115	Speer and Ribbe (1973)	Kiglapait intrusion, Labrador
28	1090	Speer and Ribbe (1973)	Kiglapait intrusion, Labrador
29	1052	Speer and Ribbe (1973)	Kiglapait intrusion, Labrador
30	303	Corlett and Eberhard (1967)	Sittampundi, India

LITERATURE

As stated by J. V. Smith (1974), many excellent summaries of the earlier literature on plagioclase optics are available, among these are Dana (1920), Winchell and Winchell (1951), Deer et al. (1963), Marfunin (1966), and Burri et al. (1967).

Prior to 1941 the optical properties of the plagioclase feldspars were considered to depend entirely upon composition. Accordingly, the observed scatter of data points around the early determinative curves for the plagioclases was attributed to errors in measuring the optical properties and, more importantly, the compositions. However, Larsson (1941) and Kohler (1942a, b) showed that some of these deviations resulted from samples having a high temperature or a low temperature origin. Later workers were thus forewarned that the optical properties of the plagioclases depended not only upon composition but also upon structural state, which proved to be the degree to which Al and Si are ordered into particular tetrahedral sites (as in "low" or ordered plagioclases) or not (as in "high" or disordered plagioclases). The later workers--notably Emmons et al. (1953), Chayes (1950, 1952, 1954), Schairer et al. (1956), J. R. Smith (1960), Urono (1963), and Balconi and Zezza (1968)--therefore attempted to reestablish the determinative curves for specimens of the same structural state.

In 1961, Burri, Parker, and Wenk selected from the literature those measurements of plagioclase optical properties and compositions that they judged to be of superior accuracy. To these they added new

data of their own to produce a monograph (Burri, Parker, and Wenk, 1967). This work presented optical data and determinative curves for specimens of both high-temperature and low-temperature origins.

Many workers, among them Federow (1893), Barth (1931), and Reinhart (1931), have plotted stereographically the positions of the two optic axes and the principal vibration directions for the plagioclases as a function of composition. Again the scatter observed in the data was attributed only to experimental error. To depict optical orientation more quantitatively Burri (1962) introduced the use of Euler angles, which are also described by Marfunin (1966), van der Plas (1966), and Burri et al. (1967).

In order to determine structural state, earlier workers relied on powder diffraction methods for determining separations of strategic peaks (Smith and Gay, 1957; Bambauer et al. (1967). However, problems arose with compositional inhomogeneity when working with the bulk samples needed for powder diffractometry. Many characteristics of the plagioclase series--such as peristeritic unmixing, coherent intergrowths, fine scale twinning, and non-Bragg 'e' and 'f' reflections-- were undetectable by these methods. Smith (1956) reported that the reciprocal lattice angle γ^* was also diagnostic of structural state and was related directly to certain peak separations (notably the 131 and $1\bar{3}1$) seen in powder patterns. Structural state could thus be determined for a single crystal and the above characteristics of the plagioclase series could be taken into account.

Ribbe (1972) demonstrated that $\Delta 2\theta \equiv 2\theta_{131}-2\theta_{1\bar{3}1}$, $\Gamma \equiv 2\theta_{131}+2\theta_{220}$

$-4\Theta_{1\bar{3}1}$, $2\Theta_{\bar{2}41}-2\Theta_{\overline{241}}$, or the cell edge, $\underline{c}$, could be used as an indicator of the amount of Al or Si ordered into particular tetrahedral sites in the plagioclase structure. A ΔAl value, based on the average Al/Si distributions was defined as the amount of Al in the T_1O site minus the average Al in the three remaining sites, T_1m, T_2O, and T_2m. This ΔAl parameter can also be used as an indicator of structural state in that for a disordered structure, the Al is randomly distributed in these four sites, thus $\Delta Al = 0$. Therefore, the larger the value of ΔAl for a specimen of a particular composition, the more ordered or the lower the structural state the specimen is.

The presence of e-diffractions, non-Bragg reflections symmetrically disposed about the $07\bar{1}$ and 093 positions in precession photographs, may also serve as an indicator of low structural state. Long term (3 days) heat treatment of intermediate plagioclases (Gay, 1956; Gay and Bown, 1956) caused the e-diffractions to decrease in intensity and eventually disappear, yet no change in the positions of the e-diffractions was detected. Foit and Peacor (1967) examined the diffraction patterns of a low intermediate plagioclase at successively higher temperatures up to 1100°C and again showed the e-diffractions to lose intensity and eventually exhibit zero intensity at a projected 1400°C. Upon cooling the e-diffractions reappeared. Smith and Ribbe (1969) attributed this phenomena to the fact that " rapid heating and cooling does not move the Si and Al atoms, which serve as a memory for persistence of the domain boundaries. As the temperature rises, geometrical differences between the domains become smaller. Furthermore, the

entropy term favors disorder, and the increased thermal vibration favors diffusion of the Na and Ca atoms. Hence, the domains become more and more similar and the subsidiary reflections fade away. Upon cooling, the framework readjusts its shape, and any diffused Na and Ca atoms tend to be pulled back again by the Si and Al atoms..."

Gay (1956) measured the separation of the e-diffractions with respect to each of the crystallographic axes. These parameters, δa, δb, and δc, were obtained following the convention of Cole et al. (1951) whereby the positions of the subsidiary layer lines containing e-diffractions were measured and related to the positions of the principal layer lines, the distance between the principal layer lines taken to be 360^{o}. Thus, if the first subsidiary layer line to be occupied is at a distance m from the zero-layer and if N is the distance between the zero- and second-layer, then the separation of the e-diffractions along that axis is (m/N) times 360^{o}.

Gay (1956) showed the separation of the e-diffractions to vary continuously and linearly with An-content. Until 1965, all data on e-diffractions was also interpreted in terms of continuous variations with respect to An-content, but Doman et al. (1965) obtained evidences of discontinuities when the separation of the e-diffractions was plotted with respect to composition, which were determined from α refractive indices and not actual analyses. Evidences of discontinuities were also present when the relations between γ^{*} and refractive indices were determined.

Various models for e-plagioclase have been proposed. Chao and

Taylor (1940) suggested a structure of alternating slabs of albite and anorthite, which ultimately is proving to be nearly correct. Megaw (1960a, b, c) considered the albite and anorthite slabs to be related by slip vectors that specify a stacking fault between the two slabs or domains. Although good in general idea, a hypothesis of this type could not adequately explain the observed Al/Si distributions or variations of intensities and positions of the e-diffractions and was ruled out by Smith and Ribbe (1969) on the basis of average T-O distances in the structure.

Smith and Ribbe (1969) developed a model " based on albite-like and anorthite-like 'domains' separated by hybrid boundary regions". They also indicated that the discontinuities were apparantly associated with particular Al-Si ratios and that " the out-of-step Al_2Si_2 and $AlSi_3$ patterns can be fitted together more easily at certain bulk ratios. Thus, there might be a different type of structure boundary for domains grown on either side of a compositional discontinuity."

Smith and Ribbe's model was essentially confirmed experimentally by Morimoto et al. (1975a, b) and Kitamura et al. (1975) by direct lattice imaging of an intermediate plagioclase exhibiting e-diffractions. High resolution TEM photographs showed alternating bands of supposed albite-like and anorthite-like structures with relatively sharp boundaries. The angle between these boundaries and a hypothetical N-S line varied for intermediate plagioclases of different compositions.

Positional and intensity variations of the e-diffractions were accounted for on the basis of a modulation wave that expresses the

shifts of all atoms in the structure, with the period of the wave thus being related to the Ca-Al/Na-Si ratio. The e-diffraction separations are related inversely to the An-content.

EXPERIMENTAL METHODS: X-RAY

Unfiltered molybdenum radiation was used to obtain $\underline{b}^*\underline{c}^*$ and $\underline{a}^*\underline{b}^*$ precession photographs. Filtered copper radiation, utilizing a 120^o oscillation such that the intensity of the diffractions was tripled for a given time period over the normal precession technique, was used to obtain $\underline{b}^*\underline{c}^*$ precession photographs on which to measure the separation of the non-Bragg subsidiary e-diffractions.

Each angular measurement of α^* and γ^* was repeated four to eight times to achieve an estimated error of less than 0.1 degree. The separation of the e-diffractions was measured with a travelling cross-hair vernier. The value, $\delta\underline{c}$, defines the separation of the e-diffractions in relation to the length of the $\underline{c}$ crystallographic axis. This parameter was measured following the convention of Cole *et al.* (1951) except that the separation was measured for a particular diffraction, $07\overline{1}$ (Figure 1), rather than groups of e-diffractions associated with particular layer lines (Figure 2).

The accuracy with which $\delta\underline{c}$ may be measured is dependent on both the separation and intensity of the e-diffractions. Reproducability of measurements for low An contents, which have less intense e-diffractions, was approximately 2-3 degrees (Figure 3), decreasing to less than 1 degree error for intense, moderately well spaced e-diffractions, and increasing again to 1-2 degrees error for e-diffractions showing only slight separation (Figures 4 and 5). One point of interest is that previous determinations of $\delta\underline{c}$ were obtained by oscillation

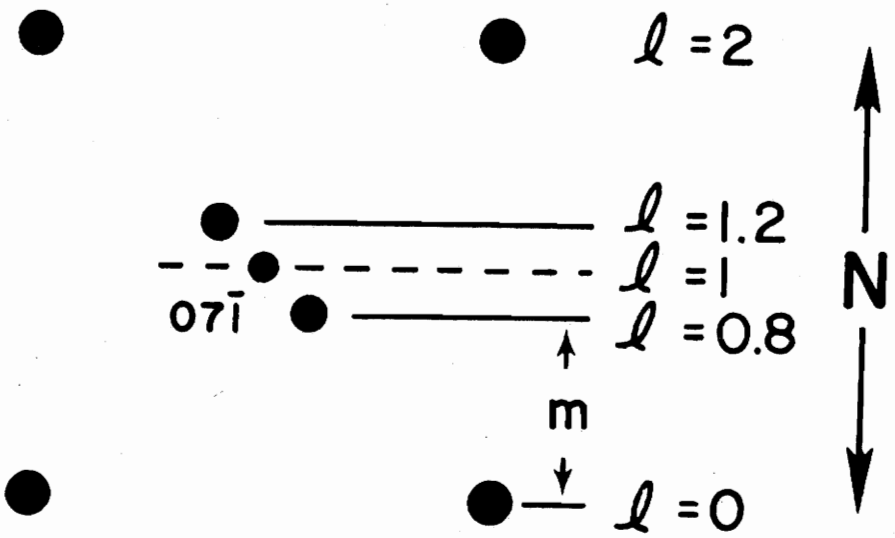

Figure 1. Measurement of δc following the modified convention of this study.

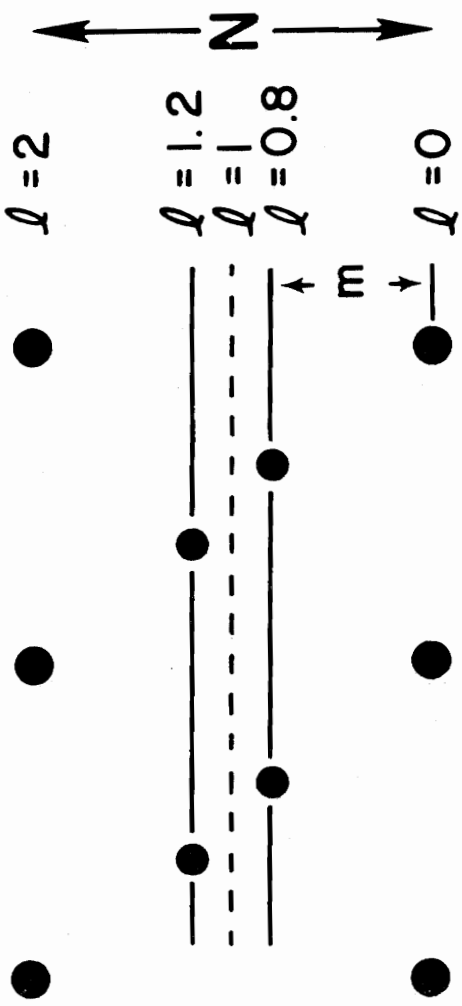

Figure 2. Measurement of δc following convention of Cole et al. (1951).

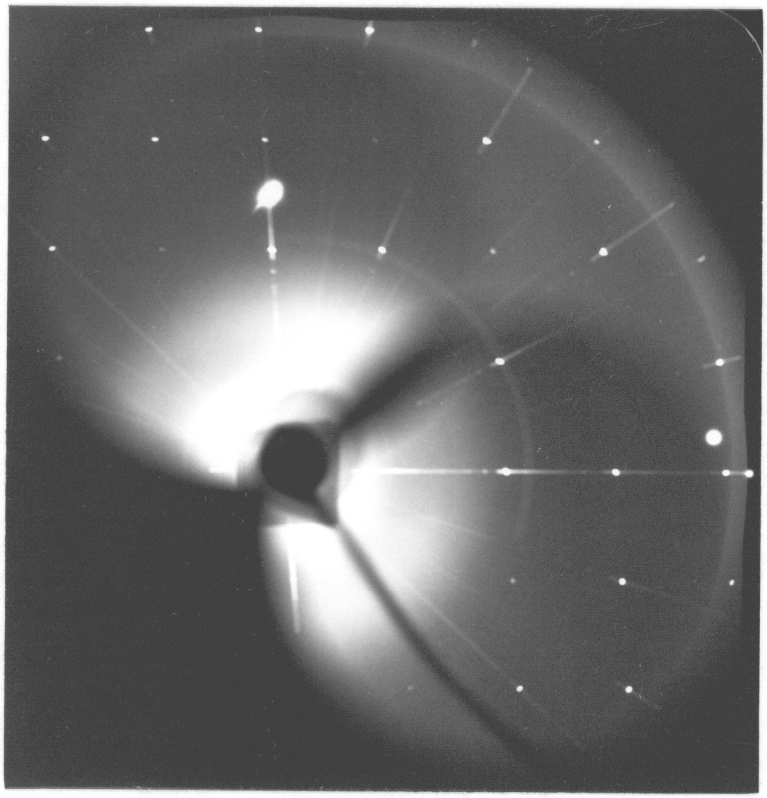

Figure 3. Precession photograph ($\underline{b}^*$ horizontal, $-\underline{c}^*$ vertical) of e-diffractions in specimen #94 ($An_{36.6}$).

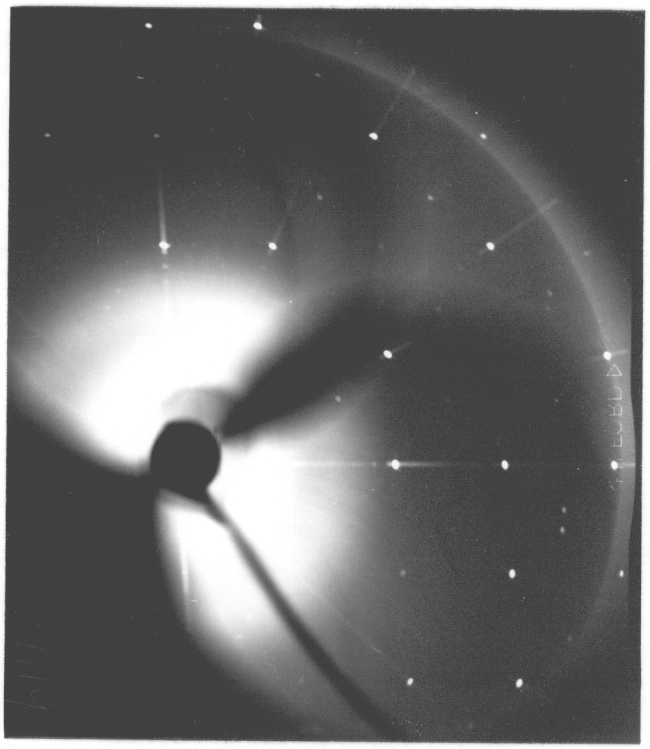

Figure 4. Precession photograph ($\underline{b}^*$ horizontal, $-\underline{c}^*$ vertical) of e-diffractions in specimen #7119 ($An_{55.0}$).

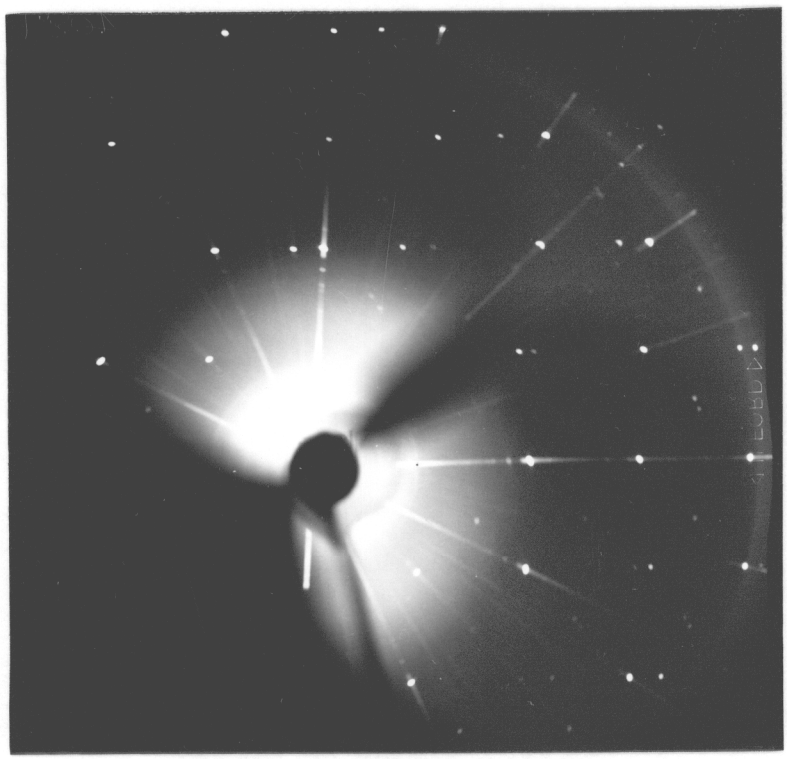

Figure 5. Precession photograph (b* horizontal, c* vertical) of e-diffractions in specimen #4087 ($An_{62.1}$).

methods for a camera of radius 30 mm compared to obtaining values by precession methods with a camera of 60 mm focal length; hence distances on the film were doubled, inherently reducing error in measurements.

EXPERIMENTAL METHODS: OPTICAL

Utilization of the Extinction Program

With the specimen cemented to a glass capillary attached to a x-ray goniometer head, a Supper spindle stage, which accepts an x-ray goniometer head, was set successively at 0 degrees, 10 degrees, 20 degrees, ... 180 degrees and the microscope stage rotated until the crystal became optically extinct. These microscope stage readings were recorded three to seven times for each spindle setting and averaged. These average values were then analyzed by least-squares computer program (Bloss and Riess, 1973) to yield spindle stage co-ordinates for the three principal vibration directions and the two optic axes, plus a value of the optic axial angle, 2V.

Cementing Agents

Initially, a 4:1 mixture of carpenter's glue and molasses served as a cementing agent (Wilcox, 1959), but as the humidity increased, the cement did not set properly thus allowing the grain to slowly change orientation. The cementing agent was then changed to clear fingernail polish in that the polish, once set, did not allow the grain to change orientation and did not affect the index of the oil in the oil cell during measurements.

Refractive Index Determination

With the co-ordinates of the principal vibration directions ob-

tained from the least-squares computer program of Bloss and Riess (1973), the refractive indices were measured by the double variation method. The spindle axis and microscope stage were set to measure the desired index and the grain then enveloped in the chosen oil in the oil cell of the spindle stage. The oil cell has provisions for variation of the temperature to thus change the oil's index and a type K, chromel-alumel thermocouple to enable the temperature of the oil to be determined from a millivolt readout on a digital Keithley 160 multimeter. A Leitz veril filter, #71736.12, served as a simple monochrometer. By means of it, a match was obtained between the refractive index of the oil and that of the grain using the Becke line method and/or a modified oblique illumination method.

The distinctiveness of the Becke line was enhanced by constricting the substage iris diaphragm and/or the iris diaphragm built into some objectives, plus increasing or decreasing the distance of the microscope objective relative to the position of sharpest focus. The opaque stop used for oblique illumination was placed directly below and against the microscope objective and moved until a shadow was seen to enter one side of the field of view thus producing a dark and light image on opposite sides of the grain. This method was enhanced by drilling a hole about 1/8th inch to 1/16th inch in diameter in the opaque stop and then observing the shadows as the grain was viewed through this hole. This, in effect, approximates the method of Wright (1913).

The Leitz veril filter has an engraved scale by which the wave-

length of match was determined. By reading the value on the right-hand side of the filter holder, the correct scale reading, called the messort number by Leitz, was recorded. At this same time the temperature equivalent millivolt value was recorded. Thus, while holding a particular temperature constant to within 0.25 degrees, the wavelength of match was recorded 5 to 12 times and averaged. The temperature of the oil was then increased approximately 2 degrees, thereby lowering the oil's index about 0.0008, and the wavelength of match again determined. After thus covering the 22 degree to 35 degree range, the oil cell was removed from the stage and its oil was replaced with the oil next to be used. The oil cell was then replaced on the microscope stage, the grain inserted into the new oil, and the spindle rotated 5 to 10 times to wash the grain of the old oil. This process was repeated three times to make sure all the previous oil was removed from both grain and cell. After the fourth insertion of the grain into the new oil, the cell and grain were ready to have the temperatures and wavelengths of match again recorded. A 10-15 minute period was allowed between the fourth oil change and when measurements were again taken to allow the cell to equilibrate to room temperature, as the cell easily conducts heat from the fingers during handling.

Each average messort number was transformed to the wavelength of match by the equation:

$$\lambda = a_1 + b_1 m + b_2 m^2 + b_3 m^3 + b_4 m^4 + b_5 m^5$$

where the six constants a_1, b_1, b_2, b_3, b_4, and b_5 were determined for filter #71736.12 by obtaining a least-squares fit to the following

calibration data supplied by Leitz for this filter:

Peak (nm)	400	450	500	550	600	650	700
m (mm)	29.7	51.8	75.2	97.7	119.4	140.6	163.7

The refractive index at a match, uncorrected for temperature, may be determined from the Hartmann equation,

$$\text{Refractive Index} = A + C/(\lambda - B)$$

where A, B, and C are the Hartmann constants determined by Bloss (The Spindle Stage, in press) for each oil, and λ is the wavelength of match. The temperature of match was determined by a first degree least-squares equation fitted to data for a type K, chromel-alumel thermocouple in the 20 degree to 40 degree C temperature range. Thus, the equation

$$\text{Index (actual)} = \text{Index (uncorrected)} + (T-25)\ dn/dt$$

where $dn/dt = -0.0004$, gives the actual index of the oil at a match.

These pairs of data points, index vs. wavelength, were then analyzed using a program, written by Louisnathan and Bloss, entitled Least Squares Dispersion Curves or simply 'LSDC' so as to yield sets of constants A, B, and C and/or n_0, m, and λ_0^2 whereby a particular principal refractive index of a grain can be calculated for any desired wavelength by use of the Hartmann equation,

$$\text{Index} = A + C/(\lambda - B)$$

or the Ketteler-Helmholtz equation,

$$\text{Index}^2 = n_0^2 + m/(\lambda_0^2 - \lambda_i^2).$$

Thermocouple Correction

While obtaining the refractive indices for the Mijakejima anorthite, rough plots of index vs. wavelength showed discrepancies between my data and previous data by Louisnathan and Bloss (1974). All thermocouple connections were checked, but new determinations still showed discrepancies. The multimeter was found to be zeroed correctly by use of an ice water bath and also produced correct millivolt equivalents for the boiling points of water and acetone. Next, another Leitz veril filter was used but values thus obtained were still in disagreement with earlier data.

In order to check whether this grain was actually exhibiting anomalous indices, and, if not, what the difference in observed and true index was, the dispersion curve of an isotropic glass of known index, Corning Glass Works #8269, was determined experimentally. These index vs. wavelength data sets were analyzed by the LSDC program. The program calculated the indices for wavelengths varying from 460 nm to 630 nm in 10 nm intervals. These values are given in Table 2 and plotted in Figure 6. If the two dispersion curves were parallel, the differences in Table 2 would be constant instead of changing from 0.001032 at 460 nm to 0.000807 at 630 nm. The amount of deviation from parallelism is thus 0.001032 minus 0.000807, i.e., 0.000225, but since this value is both within experimental error and within the error quoted for the Cargille oils, the arithmetic average of the differences was taken as a correction factor. The average difference in index was 0.000938. Since dn/dt for an oil equals about

Table 2

Indices of Refraction for Corning Glass #8269

Wavelength	Actual Index	Experimental Index	Difference
460.0	1.559367	1.560399	0.001032
470.0	1.558088	1.559119	0.001031
480.0	1.556898	1.557924	0.001026
490.0	1.556208	1.557230	0.001022
500.0	1.554751	1.555759	0.001008
510.0	1.553778	1.554775	0.000997
520.0	1.552865	1.553849	0.000984
530.0	1.552006	1.552976	0.000970
540.0	1.551197	1.552151	0.000954
550.0	1.550433	1.551372	0.000939
560.0	1.549710	1.550633	0.000923
570.0	1.549026	1.549932	0.000906
580.0	1.548377	1.549267	0.000890
590.0	1.547804	1.548678	0.000874
600.0	1.547175	1.538031	0.000856
610.0	1.546617	1.547456	0.000839
620.0	1.546085	1.546908	0.000823
630.0	1.546085	1.546908	0.000823

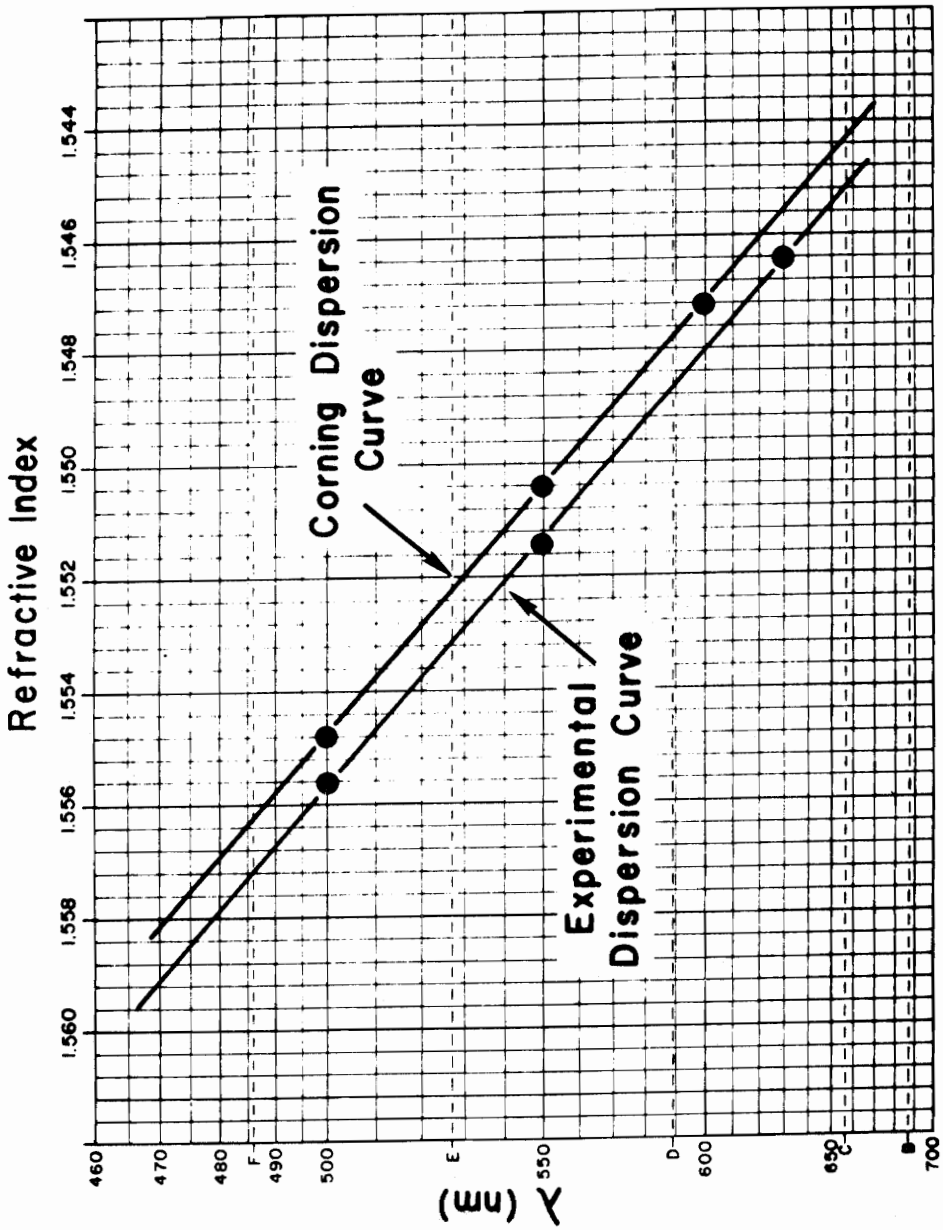

Figure 6. Dispersion curves for Corning glass #8269.

-0.0004 per degree C and since one degree C equals 0.04 millivolts in digital readout, the systematic experimental error of +0.000938 can be compensated for by adding 0.094 millivolts to the experimental millivolt readout.

Calibration of Spindle Drum Reading to Dial Axis Reading

To transfer a crystal on a goniometer head from a precession camera to a Supper spindle stage without loss of crystal orientation, the spindle setting, S, that is equivalent to a dial axis reading, D, needs to be determined. In other words, we need to determine the setting, S, that orients the crystal the same way to the light beam as the dial axis reading, D, orients the crystal to the x-ray beam. To achieve this equivalence, a glass slide was clamped to the outer arc of an x-ray goniometer head and mounted on a Supper spindle stage. The upper surface of the slide was viewed with a high power objective (32X) whose depth of focus was highly restricted. The spindle drum setting, S, was then adjusted until the upper surface of the glass slide remained in focus during extensive translation of the Supper spindle stage in the X-Y directions, where the X-Y plane parallels the plane of the microscope stage. This procedure was performed 4 to 8 times for each goniometer head and an average value taken. Without loosening the glass slide, the goniometer head was transferred to a precession camera and its dial axis rotated until the reflection of a cross from the auto-collimator beam was exactly on the crosshairs. This is the dial setting for which the auto-coll-

imator beam is exactly parallel to the x-ray beam. Since the spindle setting represents light rays perpendicular to the slide, 90 degrees must be added or subtracted to the dial axis value to also make the x-rays perpendicular to the slide. The positive difference in these two values yields a correction value which must be added to a given dial axis reading to give the setting og the spindle axis that will produce the same orientation of the crystal.

Migration Curves

The positions of the optic axes and principal vibration directions were plotted stereographically and the change in the position of each noted as the composition varied. These migration curves were plotted following the convention of Burri et al. (1967) thus relating the optic directions to the crystallographically realted directions of b*, c, and A (where A is perpendicular to b* and c). Once these directions were plotted, each inturn was rotated along small circles of the stereonet to achieve a standard orientation of the crystallographically related axes, thus b* plots along the spindle axis at S = 0 degrees and E = 0 degrees, c plots at S = 90 degrees and E = 90 degrees, and A plots at S = 180 degrees and E = 90 degrees. This study also produced a second set of migration curves such that the crystallographically related axes are now b*, C, and a (where C is perpendicular to b* and a). Again b* plots along the spindle axis at S = 0 degrees and E = 0 degrees, C plots at S = 90 degrees and E = 90 degrees, and a plots at S = 180 degrees and E = 90 degrees.

(See Appendix A for a more detailed explanation of the procedure for plotting migration curves.)

Euler Angles

Euler angles, a set of three sequential rotations whereby the crystallographically related directions are rotated into coincidence with the indicatrix, were calculated for Burri et al.'s (1967) set of crystallographically related directions (Figure 7) and for those obtained in this study (Figure 8). (See Appendix A for a more detailed explanation of the procedure for calculating Euler angles.)

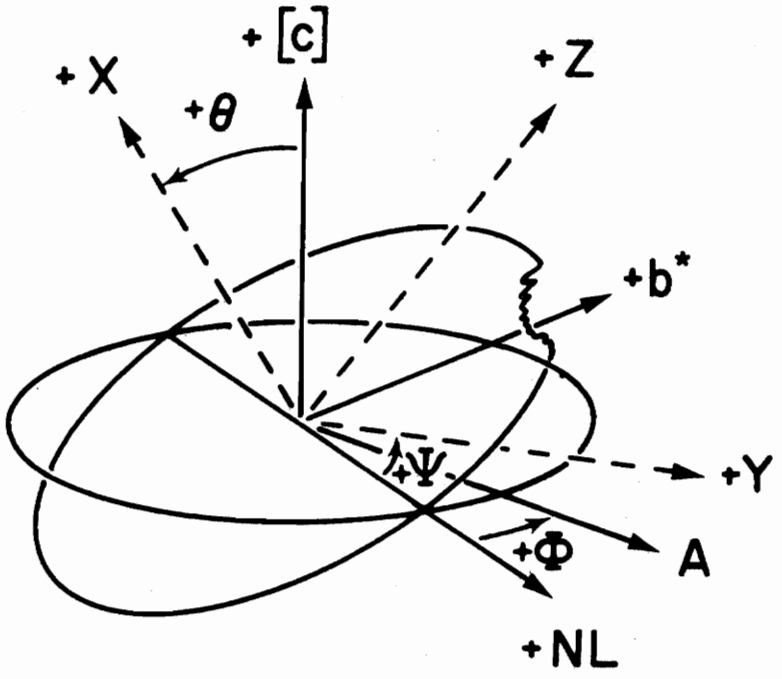

Figure 7. Euler angles Φ, Θ, and Ψ (Burri's convention)

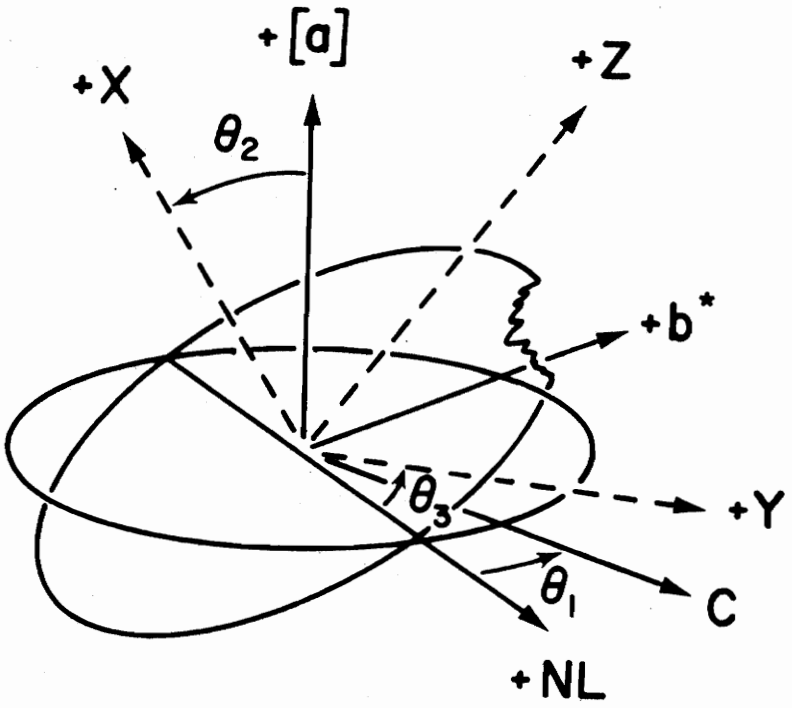

Figure 8. Euler angles Θ_1, Θ_2, and Θ_3 (Convention this study).

RESULTS AND DISCUSSION

"Inferred" Anorthite Content

The product of the three principal refractive indices, α, β, and γ, was used to determine anorthite content. These determinations were based on a first degree least-squares fit to data given by Burri et al. (1967). A correlation coefficient of 0.9997, higher than any correlation obtained by first degree fits of α, β, γ, or $\alpha+\beta+\gamma/3$ to anorthite content, was obtained for this fit of $\alpha\beta\gamma$ to anorthite content.

Bloss (1952) states that for a solid solution series in which the molar volume of the two end-members is the same or close to the same, as in the plagioclase series, density and refractive index form a linear or near linear relation, thus the close correlation of $\alpha\beta\gamma$ and anorthite content may be expected and therefore leads to the conclusion that $\alpha\beta\gamma$ should be a good indicator of anorthite content to the extent that Burri et al.'s (1967) compositions are accurate to begin with.

Determinative Curves based on Optical Parameters

Calculated curves of 2V vs. An content for this study and Burri et al. (1967) show close agreement, the maximum difference in 2V between the two curves being approximately 2.5 degrees (Table 3; Figure 9). The important point is the reduction in the scatter of data points by methods employed in this study, as compared to variations

Table 3

Observed vs. Predicted 2V Values

Inferred An%	Observed 2V	Predicted 2V	Residuals
4.1	77.09	77.60	-0.51
6.8	79.34	78.39	0.95
16.6	90.81	91.90	-1.09
27.7	96.78	96.33	0.44
30.2	97.13	94.84	2.29
30.3	96.27	94.79	1.48
35.8	86.65	89.60	-2.95
36.6	88.43	88.75	-0.32
37.6	88.07	87.67	0.39
38.7	86.02	86.50	-0.48
43.1	83.58	82.22	1.36
44.2	80.46	81.33	-0.87
44.9	82.41	80.81	1.60
48.0	78.24	79.04	-0.80
50.8	78.80	78.28	0.52
51.9	77.28	78.21	-0.93
55.0	77.69	78.68	-0.98
56.5	80.11	79.25	0.86
56.6	80.04	79.30	0.74
57.9	80.47	79.96	0.51
61.8	82.55	82.70	-0.15
62.1	81.98	82.94	-0.96
64.5	85.45	85.02	0.43
76.8	93.72	94.30	-0.58
78.2	95.38	94.84	0.53
90.4	100.59	100.61	-0.02

Figure 9. 2V vs. inferred An-content.

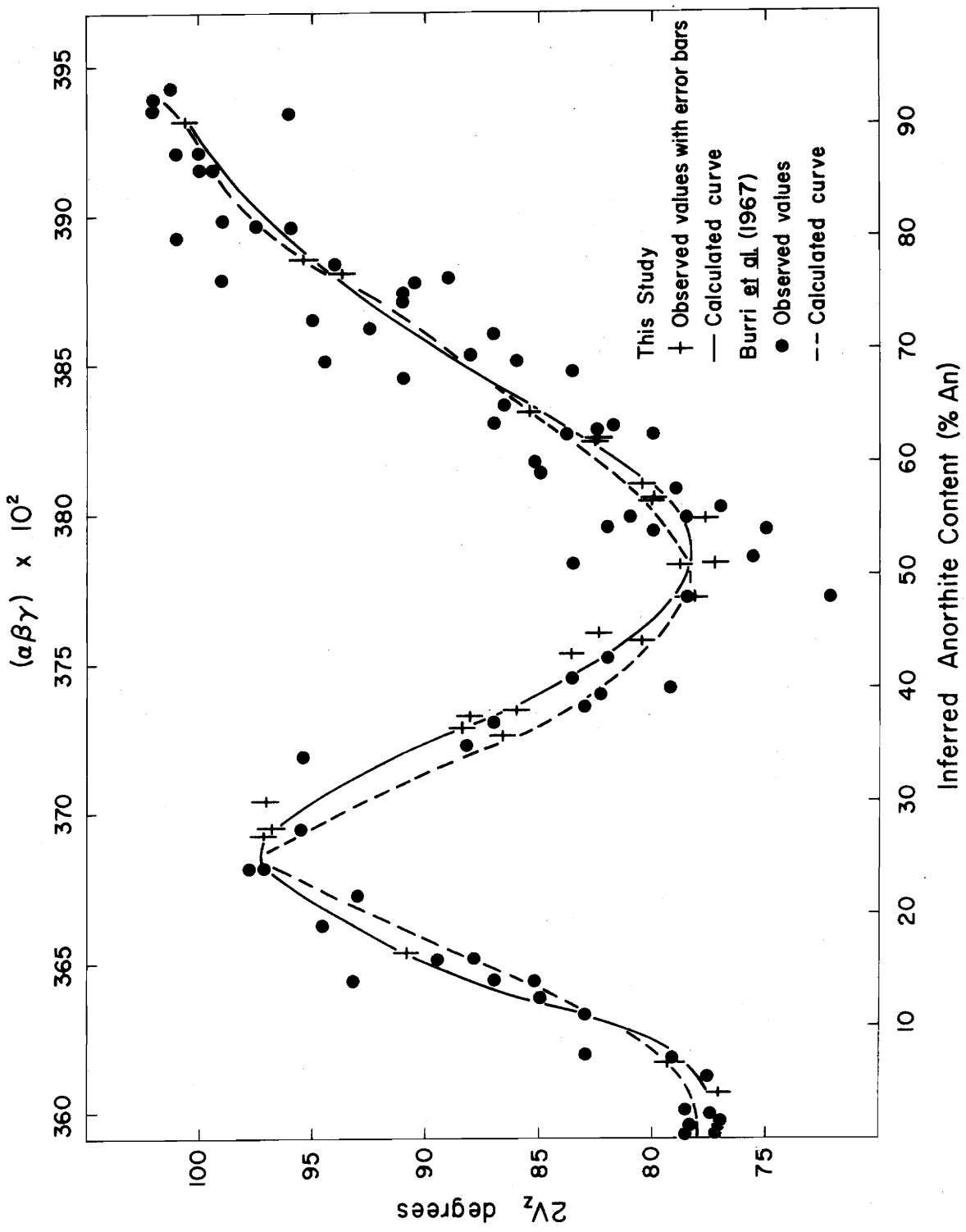
$(\alpha\beta\gamma) \times 10^2$
360
365
370
375
380
385
390
395
$2V_z$ degrees
100
95
90
85
80
75
Inferred Anorthite Content (% An)
10
20
30
40
50
60
70
80
90
This Study
+ Observed values with error bars
— Calculated curve
Burri et al. (1967)
● Observed values
-- Calculated curve

up to 10 degrees in 2V for the same or similar compositions in the study of Burri et al. (1967).

This same trend of close agreement of calculated curves accompanied by reduced scatter of the present data points is demonstrated in plots of α, β, and γ vs. An-content (Table 4; Figure 10) and of the Euler angles Φ, Θ, Ψ, Θ_1, Θ_2, and Θ_3 vs. An-content (Tables 5, 6, and 7).

Two plots of migration curves for each set of crystallographically related axes have been drafted. One depicts the calculated migration curves and the scatter of observed data about those curves for this study (Figures 11 and 12), and the other plot gives a comparison of the calculated curves for this study and the calculated curves of Burri et al. (1967) (Figures 13 and 14).

Since the positions of the two optic axes (Tables 8, 9, 10, and 11) govern the optics of the crystal, computer analysis, based on the positions of the two optic axes, was used to determine the positions of the three principal vibration directions (Tables 12 and 13). The positions of the principal vibration directions determined by polynomial regression analyses (Tables 14, 15, and 16) were not used since, by definition, these are three mutually perpendicular directions whereas the polynomial regressions did not dispose them as such.

Comparisons of the migration curves for the two studies again show very close agreement for OA2, X, Y, and Z but marked deviations for OA1 in the An 30-55 range (Figures 12 and 14). The scatter of data about the migration curves for this study is very small (Figures

Table 4

Observed vs. Predicted Refractive Indices

Inferred An%	Observed α	Predicted α	Observed β	Predicted β	Observed γ	Predicted γ
4.1	1.5292	1.5284	1.5330	1.5328	1.5387	1.5387
6.8	1.5301	1.5301	1.5344	1.5347	1.5407	1.5399
14.1	1.5343	1.5345	1.5395	1.5392	1.5430	1.5434
16.6	1.5361	1.5360	1.5404	1.5406	1.5443	1.5446
23.5	1.5399	1.5399	1.5440	1.5443	1.5477	1.5480
27.0	1.5419	1.5419	1.5458	1.5460	1.5495	1.5497
27.7	1.5418	1.5423	1.5465	1.5464	1.5500	1.5500
30.2	1.5433	1.5437	1.5477	1.5476	1.5512	1.5513
30.3	1.5429	1.5437	1.5480	1.5476	1.5515	1.5513
35.8	1.5465	1.5467	1.5506	1.5503	1.5538	1.5541
36.6	1.5469	1.5471	1.5507	1.5507	1.5546	1.5545
37.6	1.5478	1.5477	1.5511	1.5512	1.5548	1.5551
38.7	1.5481	1.5482	1.5515	1.5517	1.5558	1.5556
43.1	1.5505	1.5505	1.5537	1.5538	1.5581	1.5579
44.2	1.5512	1.5511	1.5543	1.5543	1.5585	1.5585
44.9	1.5510	1.5515	1.5549	1.5547	1.5593	1.5589
48.0	1.5533	1.5530	1.5560	1.5562	1.5606	1.5605
50.8	1.5549	1.5544	1.5576	1.5576	1.5618	1.5620
51.9	1.5555	1.5549	1.5581	1.5582	1.5622	1.5626
55.0	1.5564	1.5565	1.5599	1.5598	1.5645	1.5642
56.5	1.5573	1.5572	1.5607	1.5606	1.5651	1.5651
56.6	1.5576	1.5572	1.5606	1.5606	1.5650	1.5651
57.9	1.5584	1.5578	1.5613	1.5613	1.5656	1.5658
59.5	1.5587	1.5586	1.5620	1.5621	1.5670	1.5667
61.8	1.5597	1.5597	1.5632	1.5634	1.5683	1.5680

Table 4 (con't)

62.1	1.5601	1.5598	1.5635	1.5635	1.5681	1.5681
64.5	1.5609	1.5609	1.5650	1.5648	1.5695	1.5695
76.8	1.5656	1.5663	1.5718	1.5717	1.5768	1.5764
78.2	1.5669	1.5669	1.5724	1.5725	1.5770	1.5772
90.4	1.5716	1.5718	1.5791	1.5791	1.5841	1.5844

Figure 10. α, β, and γ vs. inferred An-content.

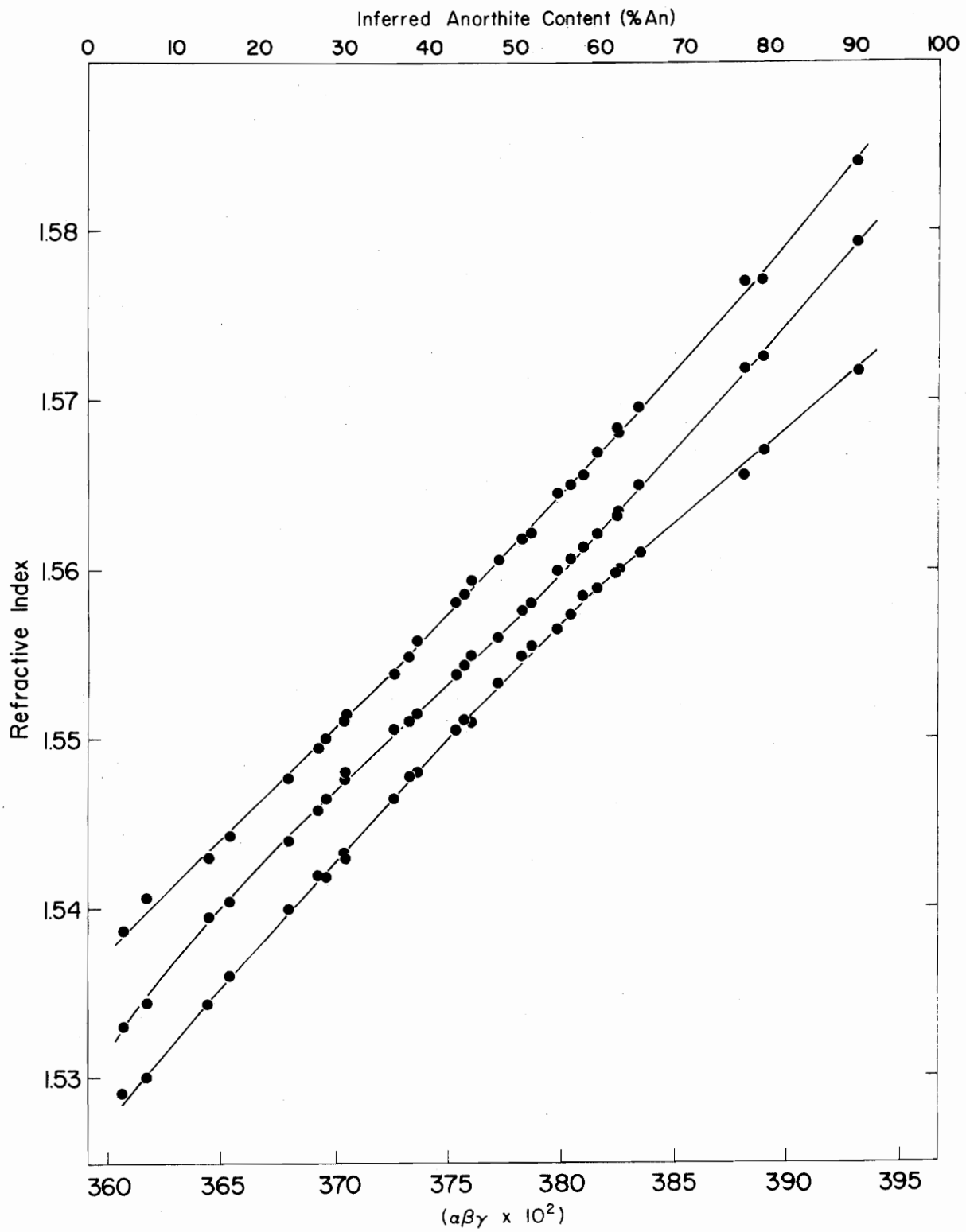
Inferred Anorthite Content (%An)
0
10
20
30
40
50
60
70
80
90
100
Refractive Index
1.58
1.57
1.56
1.55
1.54
1.53
360
365
370
375
380
385
390
395
(αβγ x 10²)

Table 5

Observed vs. Predicted Euler Angles (Burri Convention)

Inferred An%	Observed Φ	Predicted Φ	Observed Θ	Predicted Θ	Observed Ψ	Predicted Ψ
4.1	88.84	89.05	83.20	82.56	106.47	106.38
6.8	89.72	89.21	82.73	83.86	104.19	104.70
16.6	90.79	90.98	72.12	70.86	95.88	94.50
27.7	90.05	91.21	61.61	63.72	79.10	80.70
30.2	90.26	90.59	64.09	62.92	79.02	77.61
35.8	88.63	87.98	59.80	60.07	69.10	70.72
36.6	87.25	87.47	58.76	59.48	68.95	69.73
37.6	86.46	86.78	58.48	58.66	67.42	68.48
38.7	86.38	85.95	58.89	57.70	66.02	67.09
43.1	82.64	81.95	53.66	52.94	62.49	61.40
44.2	81.67	80.78	50.49	51.59	61.88	59.92
48.0	78.52	76.26	48.70	46.72	56.10	54.58
50.8	75.13	72.48	44.37	43.22	53.26	50.39
51.9	71.54	70.89	40.79	41.94	50.92	48.67
55.0	62.35	66.19	37.86	38.76	41.37	43.63
56.5	61.56	63.80	37.90	37.51	39.59	41.07
56.6	61.48	63.64	36.05	37.43	39.09	40.89
57.9	58.77	61.51	35.09	36.54	36.97	38.61
61.8	54.80	54.95	36.53	34.88	30.67	31.46
62.1	56.32	54.44	35.13	34.81	30.99	30.90
64.5	53.32	50.33	34.77	34.56	27.89	26.30
76.8	31.04	31.33	35.47	35.49	3.27	3.40
78.2	30.17	29.68	35.13	35.19	1.92	1.26
90.4	24.59	24.81	38.34	38.32	-3.76	-3.60

Table 6

Observed vs. Predicted Euler Angles (Convention this study)

Inferred An%	Observed Θ_1	Predicted Θ_1	Observed Θ_2	Predicted Θ_2	Observed Θ_3	Predicted Θ_3
4.1	175.48	175.31	73.97	74.55	-19.77	-17.34
6.8	175.58	176.07	76.46	75.40	-17.11	-17.16
16.6	178.39	178.32	84.54	85.46	-8.86	-13.30
27.7	179.59	179.91	100.91	100.10	-2.03	-4.03
30.2	179.81	180.12	101.19	103.01	0.20	-1.40
35.8	179.74	180.42	110.25	108.67	4.17	5.04
36.6	180.27	180.45	109.76	109.38	6.65	6.01
37.6	181.21	180.47	110.91	110.23	5.10	7.24
38.7	180.98	180.48	112.29	111.12	5.58	8.61
43.1	181.47	180.43	113.80	114.27	11.12	14.26
44.2	180.14	180.39	113.64	114.97	15.83	15.70
48.0	181.12	180.18	117.54	117.15	16.55	20.74
50.8	179.84	179.95	117.84	118.60	22.94	24.48
51.9	179.65	179.84	117.44	119.15	27.43	25.95
55.0	180.39	179.49	120.65	120.66	33.21	30.06
56.5	180.18	179.29	121.69	121.39	33.49	32.03
56.6	178.29	179.27	121.41	121.44	35.86	32.17
57.9	178.61	179.08	121.40	122.08	37.53	33.86
61.8	179.39	178.43	125.39	124.07	37.39	38.82
62.1	179.22	178.37	125.18	124.23	35.00	39.20
64.5	176.38	177.90	125.85	125.55	41.57	42.13
76.8	171.82	174.74	132.96	133.01	56.78	55.10
78.2	172.41	174.30	133.12	133.80	57.14	56.29
90.4	172.04	169.79	135.89	135.74	62.01	63.29

Table 7

Euler Angles Θ_1, Θ_2, and Θ_3 for Burri's Data

Inferred An%	Θ_1	Θ_2	Θ_3
0.0	174.80	74.27	-20.86
5.0	176.66	75.15	-19.44
10.0	177.04	78.82	-15.90
15.0	177.99	83.31	-11.15
20.0	178.70	89.31	-5.83
25.0	179.80	97.71	-1.57
30.0	179.90	105.41	0.96
35.0	180.11	108.31	4.97
40.0	180.22	111.51	11.02
45.0	180.77	114.30	17.07
50.0	180.90	116.81	23.38
55.0	180.69	119.30	30.25
60.0	178.33	121.24	37.28
65.0	177.25	126.77	43.40
70.0	175.19	129.61	49.66
75.0	174.69	130.98	51.36
80.0	172.95	133.49	55.18
85.0	171.44	135.38	60.13
90.0	172.25	135.74	60.69
92.5	171.61	136.09	62.18

Figure 11. Observed data vs. calculated migration curves (Burri's convention).

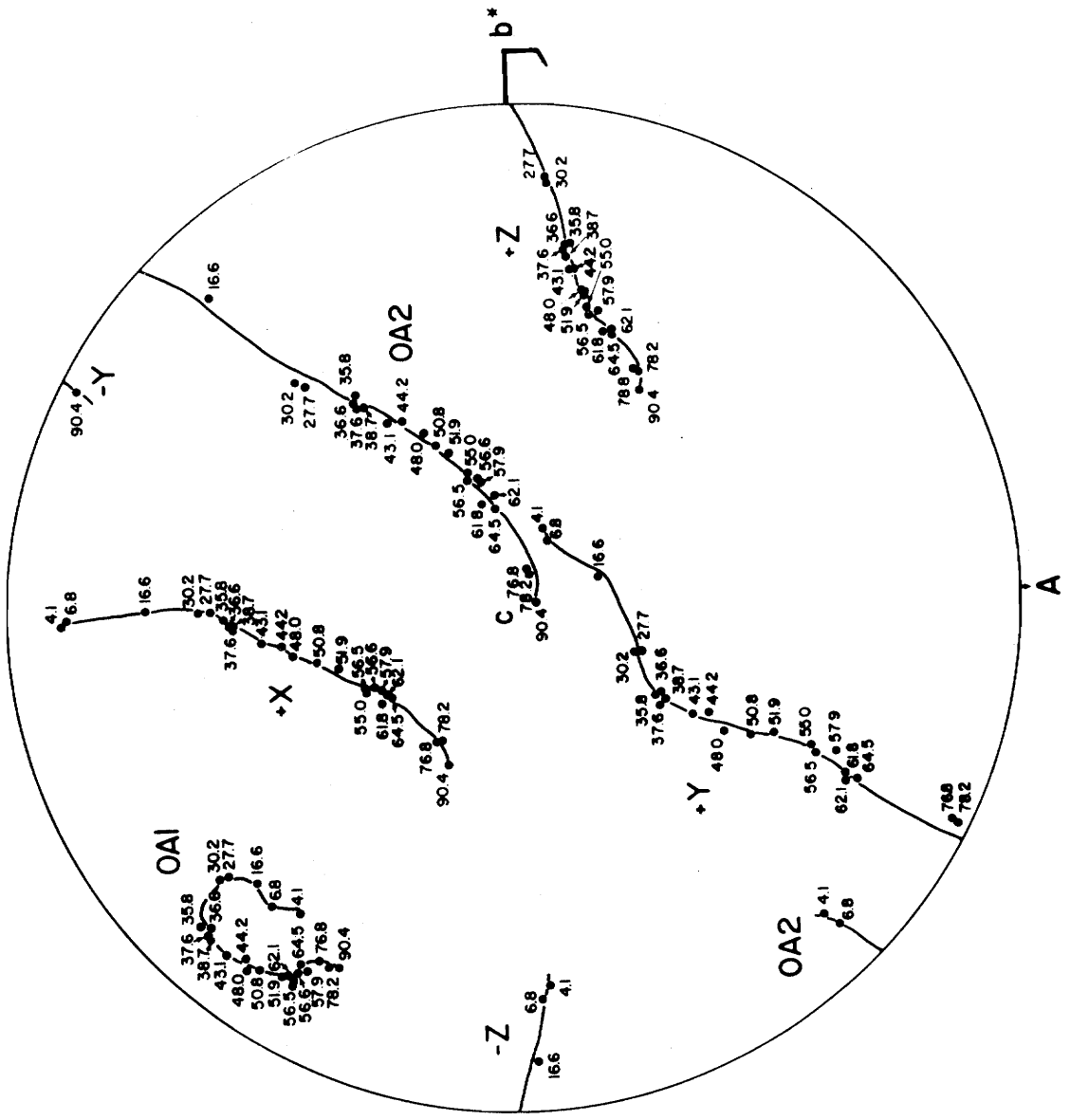
b*
A
+Z
-Y
OA2
+X
C
+Y
OA1
-Z
OA2

Figure 12. Calculated migration curves for this study vs. calculated migration curves of Burri *et al.* (1967).

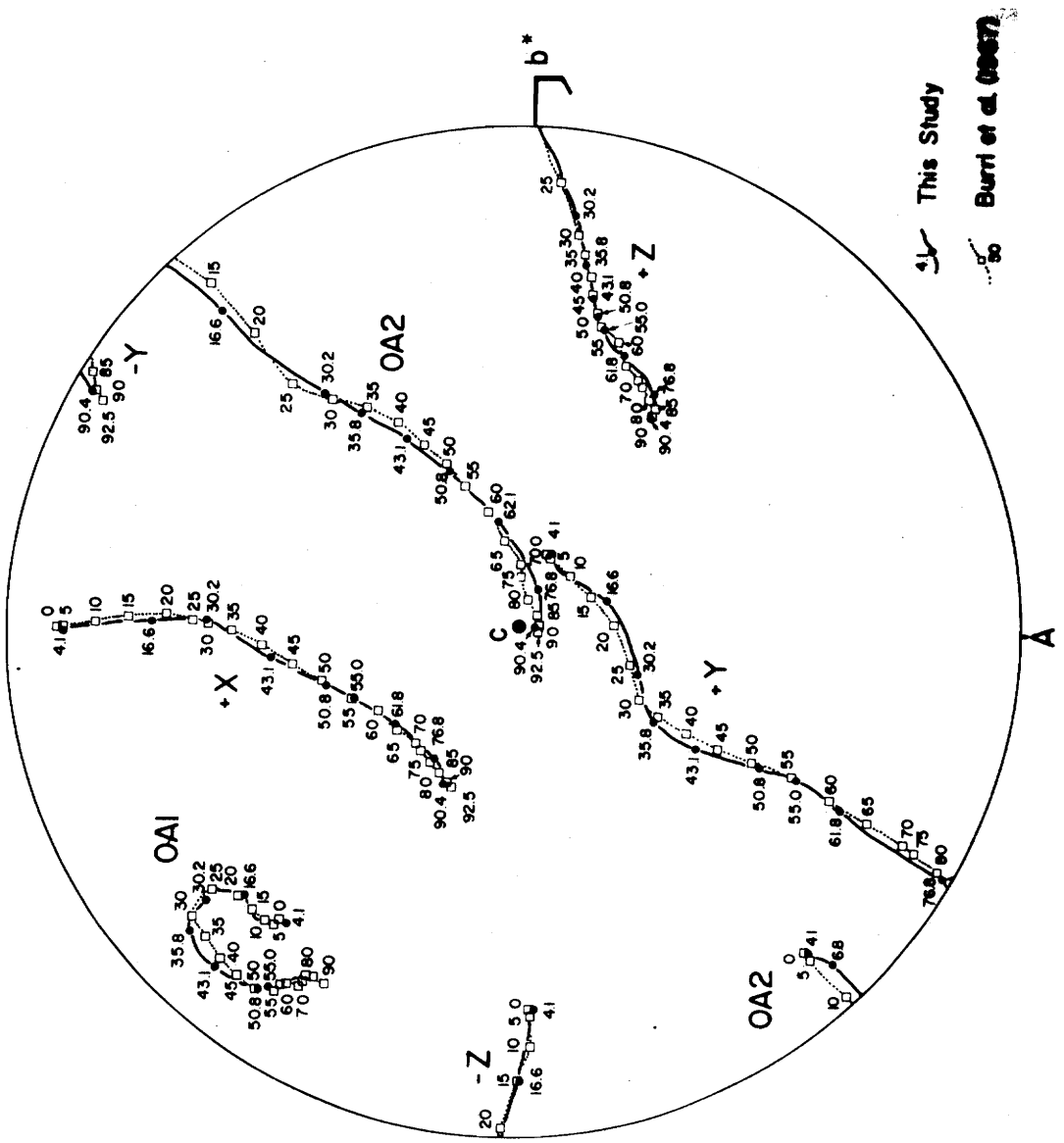
b*
A
+Z
+Y
+X
-Y
-Z
OA1
OA2
OA2
C
This Study
Burri et al. (1967)

Figure 13. Observed data vs. calculated migration curves (Convention this study).

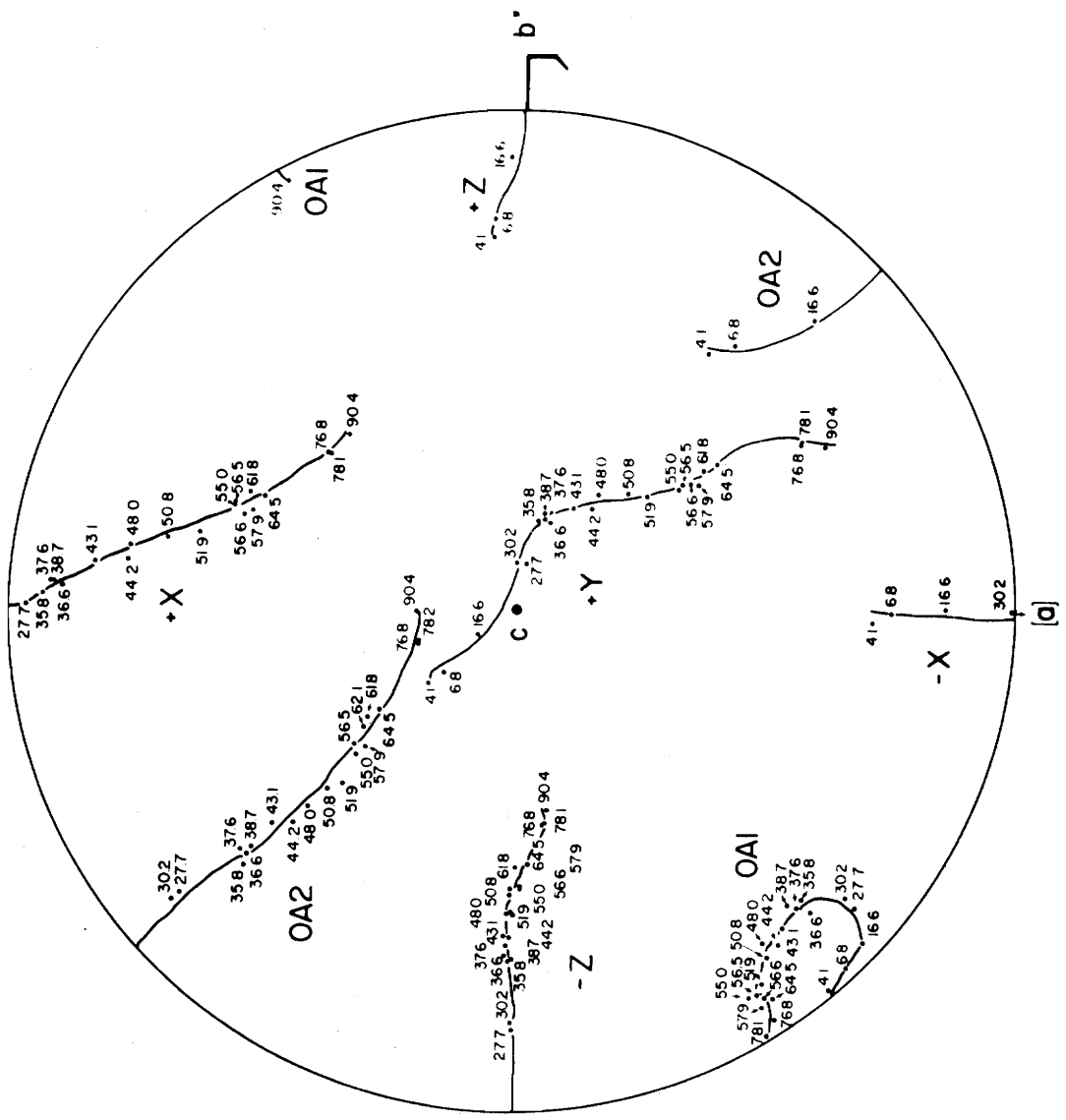
b'
OA1
+Z
OA2
+X
+Y
c
-Z
OA1
OA2
-X
[a]

Figure 14. Calculated migration curves for this study vs. calculated migration curves of Burri *et al.* (1967).

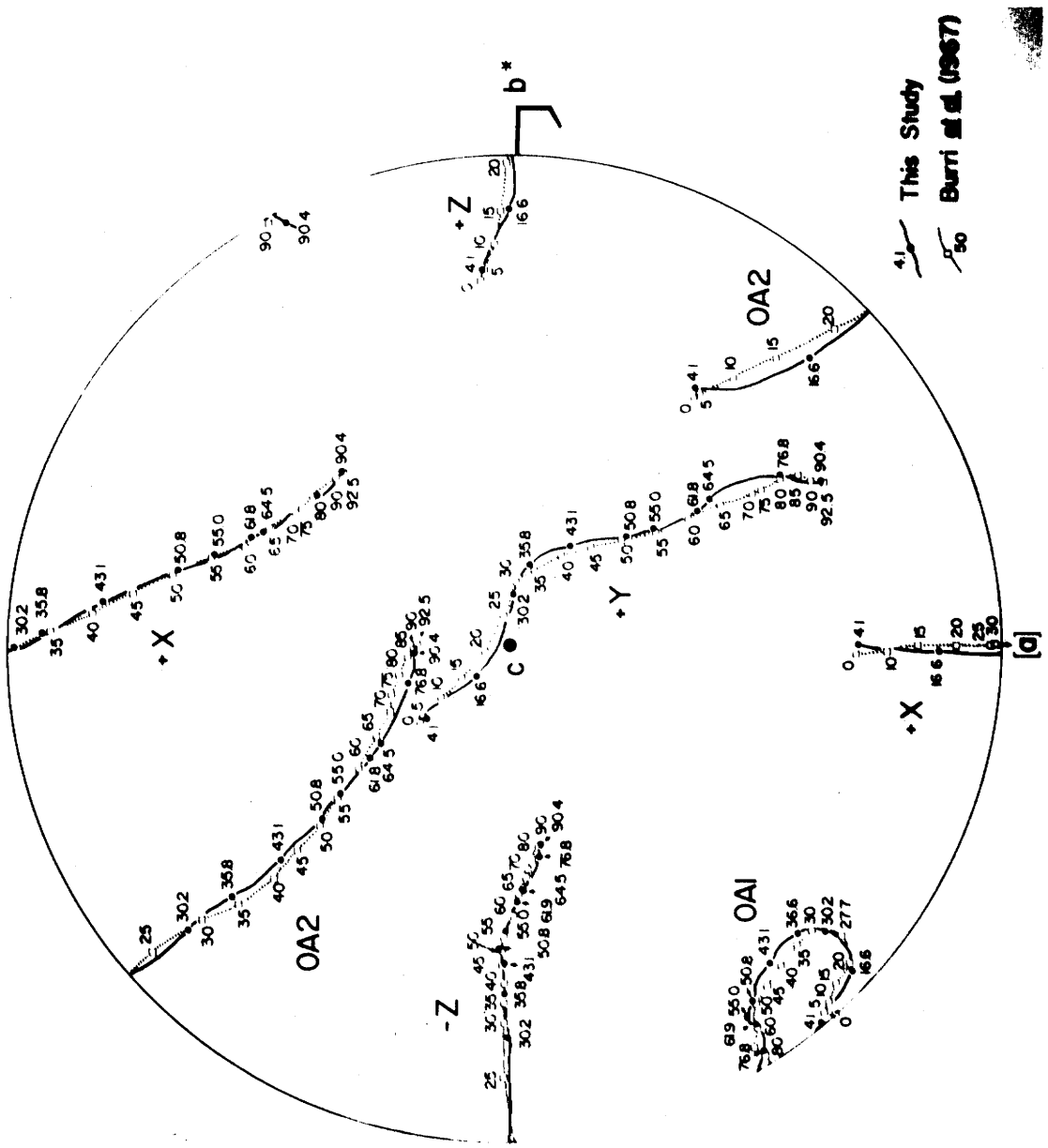
This Study
Burri et al. (1967)
b*
+Z
+X
+Y
-Z
OA2
OA1
C
[a]

Table 8

Observed vs. Predicted Values of S and E for OAl
(Burri's Convention)

Inferred An%	Observed S	Predicted S	Observed E	Predicted E
4.1	27.24	27.67	139.97	139.94
6.8	23.09	22.30	137.22	137.29
16.6	23.93	22.82	133.24	133.07
27.7	18.85	18.43	130.66	130.75
30.2	17.30	15.92	130.38	131.12
35.8	9.97	11.52	133.81	133.53
36.6	11.49	11.12	134.67	134.03
37.6	10.44	10.72	135.07	134.71
38.7	10.05	10.40	135.51	135.50
43.1	10.22	10.37	138.65	139.00
44.2	12.09	10.63	140.50	139.89
48.0	10.57	12.13	141.92	142.79
50.8	12.48	13.55	142.86	144.55
51.9	15.06	14.12	145.50	145.12
55.0	15.28	15.61	147.08	146.28
56.5	15.58	16.21	147.09	146.60
56.6	17.91	16.25	146.51	146.62
57.9	19.37	16.70	147.56	146.76
61.8	15.48	17.61	147.04	146.64
62.1	16.16	17.66	145.99	146.60
64.5	18.87	17.98	145.79	146.23
76.8	24.31	23.70	147.33	147.54
78.2	24.82	25.30	148.75	148.48
90.4	26.52	26.54	149.80	149.82

Table 9

Observed vs. Predicted Values of S and E for OA2

Inferred An%	Observed S	Predicted S	Observed E	Predicted E
4.1	168.27	167.18	136.80	137.59
6.8	171.60	172.75	136.22	136.00
16.6	12.34	12.66	44.27	44.72
27.7	37.95	34.14	49.27	47.61
30.2	35.62	38.73	49.18	47.91
35.8	49.73	48.60	48.29	49.03
36.6	49.65	49.96	49.77	49.26
37.6	50.80	51.64	50.60	49.57
38.7	52.14	53.46	50.23	49.94
43.1	58.34	60.46	52.17	51.78
44.2	62.14	62.13	51.16	52.34
48.0	67.47	67.65	53.06	54.57
50.8	70.94	71.46	55.30	56.52
51.9	74.34	72.89	56.43	57.35
55.0	78.64	76.71	60.57	59.88
56.5	78.81	78.45	62.41	61.20
56.6	80.85	78.56	61.70	61.29
57.9	81.66	80.00	62.69	62.48
61.8	82.69	83.95	67.28	66.26
62.1	84.68	84.23	65.52	66.57
64.5	84.76	86.35	68.44	69.03
76.8	92.16	93.46	82.08	81.66
78.2	92.49	93.84	83.15	82.93
90.4	94.16	92.98	89.50	89.73

Table 10

Observed vs. Predicted Values of S and E for OA1
(Convention this study)

Inferred An%	Observed S	Predicted S	Observed E	Predicted E
4.1	178.76	179.63	139.97	139.91
6.8	178.05	178.45	136.68	136.81
16.6	177.23	177.95	133.24	133.00
27.7	172.45	171.36	130.66	130.85
30.2	170.17	168.91	130.38	131.16
35.8	163.67	164.87	133.81	133.48
36.6	166.54	164.53	134.67	133.98
37.6	163.64	164.19	135.07	134.66
38.7	162.05	163.94	135.51	135.45
43.1	163.87	164.09	138.65	138.99
44.2	165.84	164.37	140.50	139.91
48.0	162.32	165.83	141.92	142.89
50.8	166.38	167.14	142.86	144.69
51.9	169.06	167.65	145.50	145.28
55.0	169.28	168.94	148.08	146.45
56.5	169.38	169.45	147.09	146.77
56.6	171.91	169.48	146.51	146.79
57.9	173.37	169.85	147.60	146.91
61.8	168.48	170.57	147.04	146.69
62.1	166.15	170.61	145.99	146.64
64.5	172.87	170.88	145.79	146.18
76.8	177.36	177.33	147.33	147.47
78.2	179.24	179.08	148.75	148.54
90.4	183.03	183.02	151.79	151.82

Table 11

Observed vs. Predicted Values of S and E for OA2
(Convention this study)

Inferred An%	Observed S	Predicted S	Observed E	Predicted E
4.1	141.27	141.43	42.20	41.38
6.8	147.66	146.96	42.88	43.42
16.6	166.64	166.73	45.27	46.98
27.7	11.55	8.05	130.73	132.09
30.2	9.12	12.60	130.82	131.84
35.8	23.43	22.40	131.71	130.86
36.6	24.70	23.75	130.23	130.66
37.6	24.00	25.41	129.40	130.38
38.7	26.14	27.22	129.77	130.04
43.1	31.99	34.17	127.83	128.29
44.2	36.89	35.82	128.84	127.76
48.0	40.42	41.32	126.94	125.58
50.8	44.84	45.09	124.70	123.65
51.9	48.34	46.52	124.57	122.82
55.0	52.64	50.33	119.43	120.29
56.5	52.61	52.05	117.59	118.96
56.6	54.85	52.17	118.20	118.87
57.9	55.66	53.60	117.31	117.67
61.8	55.69	57.54	112.72	113.83
62.1	54.68	57.82	114.48	113.52
64.5	58.76	59.94	111.56	111.01
76.8	67.21	67.13	97.92	98.14
78.2	66.93	67.53	96.85	96.85
90.4	67.47	66.90	90.50	90.40

Table 12

Calculated Co-ordinates of AB, ON, and OB based on Calculated Positions of Optic Axes (Burri's Convention)

	AB		ON		OB	
Inferred An%	S	E	S	E	S	E
4.1	101.05	163.09	96.56	73.14	6.93	91.25
6.8	100.10	166.44	97.18	76.46	7.33	90.66
16.6	107.82	173.55	108.78	83.55	18.76	89.89
27.7	121.58	9.80	116.04	99.76	26.18	89.16
30.2	119.46	12.57	117.12	102.56	27.23	89.50
35.8	116.59	19.34	120.93	109.27	30.45	91.35
36.6	116.29	20.07	121.70	109.99	31.06	91.74
37.6	115.93	20.92	122.78	110.81	31.91	92.28
38.7	115.58	21.76	124.08	111.55	32.92	92.92
43.1	114.53	24.35	130.41	113.53	37.81	95.94
44.2	114.37	24.88	132.22	113.82	39.21	96.77
48.0	114.18	26.53	138.82	114.41	44.34	99.76
50.8	114.52	27.79	143.76	114.70	48.18	101.94
51.9	114.70	28.30	145.69	114.81	49.66	102.80
55.0	115.88	29.99	150.77	115.34	53.49	104.98
56.5	116.62	30.92	153.10	115.72	55.17	105.98
56.6	116.66	30.98	153.25	115.74	55.28	106.04
57.9	117.40	31.84	155.18	116.15	56.62	106.86
61.8	119.90	34.76	160.60	117.76	60.04	109.20
62.1	120.10	34.98	160.98	117.88	60.26	109.37
64.5	121.69	36.92	164.07	119.04	61.94	110.73
76.8	125.53	43.81	178.62	119.95	70.26	118.65

Table 12 (con't)

78.2	125.12	43.86	179.93	118.98	71.49	119.68
90.4	125.12	43.86	179.93	118.98	71.49	119.68

Table 13

Calculated Co-ordinates of AB, ON, and OB based on Calculated Positions of Optic Axes (Convention this study)

	AB		ON		OB	
Inferred An%	S	E	S	E	S	E
4.1	72.70	15.76	70.46	105.75	160.27	89.32
6.8	72.17	13.50	71.68	103.50	161.66	89.89
16.6	82.71	6.51	82.82	96.51	172.84	90.12
27.7	93.43	170.66	90.29	80.67	0.39	90.63
30.2	92.18	166.93	90.52	76.93	0.60	90.35
35.8	90.14	160.41	94.53	70.46	4.04	88.62
36.6	89.90	159.71	95.33	69.79	4.68	88.24
37.6	89.59	158.92	96.43	69.05	5.55	87.72
38.7	89.29	158.12	97.74	68.33	6.58	87.10
43.1	88.30	155.67	104.10	66.48	11.52	84.11
44.2	88.12	155.19	105.81	66.23	12.83	83.28
48.0	87.83	153.58	112.48	65.69	18.04	80.28
50.8	88.06	152.32	117.38	65.42	21.83	78.07
51.9	88.29	151.78	119.26	65.29	23.27	77.24
55.0	89.34	150.05	124.33	64.73	27.06	75.01
56.5	90.05	149.10	126.63	64.33	28.70	74.00
56.6	90.10	149.03	126.80	64.30	28.82	73.93
57.9	90.83	148.14	128.70	63.86	30.12	73.10
61.8	93.37	145.14	134.06	62.15	33.44	70.77
62.1	93.58	144.90	134.45	62.01	33.66	70.60
64.5	95.22	142.88	137.54	60.76	35.29	69.25
76.8	99.23	136.04	152.39	59.96	43.90	61.27

Table 13 (con't)

78.2	98.74	136.06	153.73	61.06	45.25	60.19
90.4	97.61	133.92	158.38	63.11	48.16	55.71

Table 14

Observed vs. Predicted Values of S and E for AB(Z)
(Burri's Convention)

Inferred An%	Observed S	Predicted S	Observed E	Predicted E
4.1	101.67	103.01	163.36	165.41
6.8	98.38	95.91	165.77	166.86
16.6	100.36	103.25	174.31	168.80
27.7	118.62	115.38	10.92	13.60
30.2	117.08	116.10	11.09	14.67
35.8	117.01	115.88	20.25	17.59
36.6	114.70	115.73	19.76	18.06
37.6	113.64	115.52	20.94	18.66
38.7	113.60	115.29	22.31	19.34
43.1	113.01	114.50	23.84	22.23
44.2	114.92	114.39	23.64	22.99
48.0	114.91	114.44	27.56	25.68
50.8	116.40	114.97	27.84	27.71
51.9	116.67	115.28	27.44	28.52
55.0	115.34	116.45	30.65	30.78
56.5	115.91	117.13	31.69	31.86
56.6	118.79	117.18	31.45	31.93
57.9	118.27	117.82	31.43	32.86
61.8	117.86	119.85	35.39	35.58
62.1	121.10	120.00	35.19	35.78
64.5	120.99	121.17	36.01	37.36
76.8	122.60	123.13	43.44	43.89
78.2	123.59	122.87	43.65	44.41
90.4	123.10	123.11	47.42	46.13

Table 15

Observed vs. Predicted Values of S and E for ON(Y)
(Burri's Convention)

Inferred An%	Observed S	Predicted S	Observed E	Predicted E
4.1	96.46	97.15	73.40	74.02
6.8	97.20	95.96	75.77	74.70
16.6	107.96	109.23	84.36	85.07
27.7	117.39	115.86	100.92	100.31
30.2	115.88	116.73	101.09	103.23
35.8	120.65	120.31	110.21	108.65
36.6	122.11	121.08	109.61	109.29
37.6	122.71	122.14	110.70	110.04
38.7	122.42	123.43	112.07	110.81
43.1	129.09	129.82	113.00	113.26
44.2	132.50	131.67	112.65	113.73
48.0	135.99	138.54	115.96	115.00
50.8	141.62	143.77	115.54	115.64
51.9	146.18	145.77	114.32	115.84
55.0	153.42	151.19	115.00	116.27
56.5	154.15	153.60	115.99	116.42
56.6	155.37	153.76	116.08	116.44
57.9	157.51	155.71	115.34	116.56
61.8	159.92	160.82	117.81	116.90
62.1	160.27	161.17	118.67	116.93
64.5	162.30	163.76	118.64	117.16
76.8	177.85	177.12	118.36	118.89
78.2	178.74	179.08	118.59	119.08
90.4	2.90	2.87	62.70	62.87

Table 16

Observed vs. Predicted Values of S and E for OB(X)
(Burri's Convention)

Inferred An%	Observed S	Predicted S	Observed E	Predicted E
4.1	6.80	8.05	91.15	91.91
6.8	7.27	8.72	90.28	90.37
16.6	17.88	13.68	89.25	87.58
27.7	28.39	23.04	89.96	88.91
30.2	25.91	25.53	89.77	89.75
35.8	30.21	31.46	91.18	92.19
36.6	31.27	32.33	92.35	92.59
37.6	31.57	33.43	93.02	93.11
38.7	31.16	34.65	93.10	93.71
43.1	36.57	39.59	95.92	96.32
44.2	39.81	40.83	96.42	97.02
48.0	41.88	45.09	98.60	99.53
50.8	46.61	48.19	100.34	101.48
51.9	50.70	49.39	101.94	102.25
55.0	55.45	52.70	106.55	104.48
56.5	55.61	54.25	107.01	105.56
56.6	57.40	54.36	106.32	105.63
57.9	59.01	55.67	107.34	106.58
61.8	58.81	59.44	110.07	109.40
62.1	59.65	59.71	108.61	109.62
64.5	60.89	61.85	109.92	111.32
76.8	69.83	70.15	119.81	119.19
78.2	70.53	70.75	119.83	119.95
90.4	71.78	72.13	124.34	124.60

11 and 13) and, based on the scatter in 2V for Burri et al.'s (1967) curve, one may conclude the scatter of Burri et al.'s (1967) data for migration curves to be greater than this study.

Examination of the observed migration curves shows the positions of OA2, X, and Y to be reversed for samples of $An_{27.7}$ and $An_{30.2}$, thus indicating the possibility the migration curves may also be segmented rather than continuous curves, although many more determinations of samples in this region need be examined for conclusive proof. In the region An_{48-50}, where the second discontinuity exists, no other such reversals were evident.

Relation of γ^* to An-content and Refractive Indices

The discontinuities observed by Doman et al. (1965) in plots of γ^* vs. α, β, γ, and An-content are confirmed by this study (Figure 15). However, Doman et al. (1965) report discontinuities at approximately An_{33} and An_{50}, whereas this study yields breaks at approximately An_{30} and An_{45-48}. This, the writer feels, may be a consequence of not yet having a complete microprobe analysis for grains of this study, in that, along with Na and Ca affecting refractive indices, the effect of K and/or trace elements (Fe, Ba, Ti) on the refractive indices is yet to be determined.

An attempt was made to determine statistically whether these discontinuities were real or the result of errors in data collection. For each of the four curves (Figures 15 and 16), a linear equation was fit to each segment of the curve and then to all the data for that

Figure 15. γ^* vs. inferred An-content.

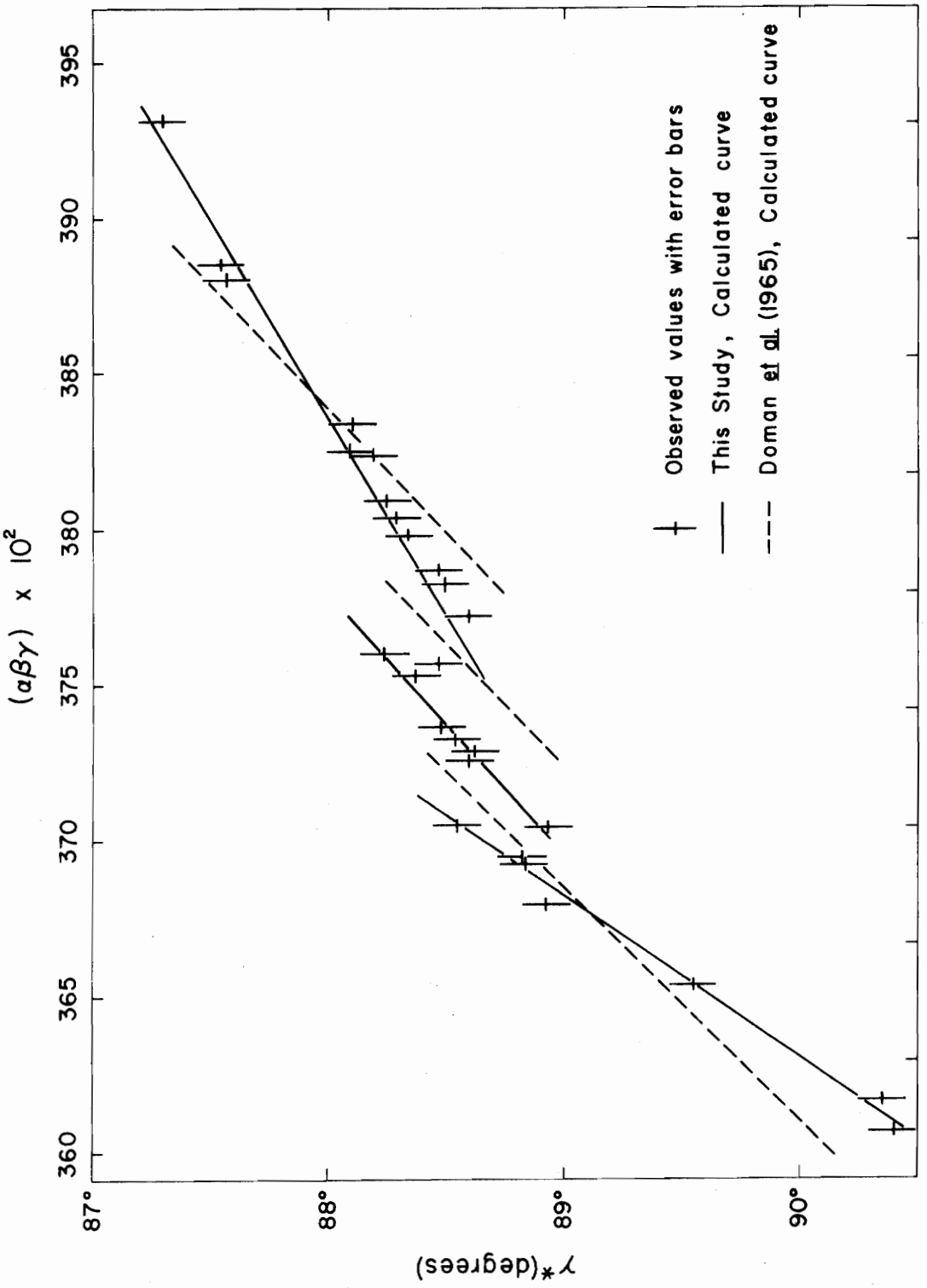
$(\alpha\beta\gamma) \times 10^2$
360
365
370
375
380
385
390
395
γ^*(degrees)
87°
88°
89°
90°
Inferred Anorthite Content (% An)
10
20
30
40
50
60
70
80
90
Observed values with error bars
This Study, Calculated curve
Doman et al (1965), Calculated curve

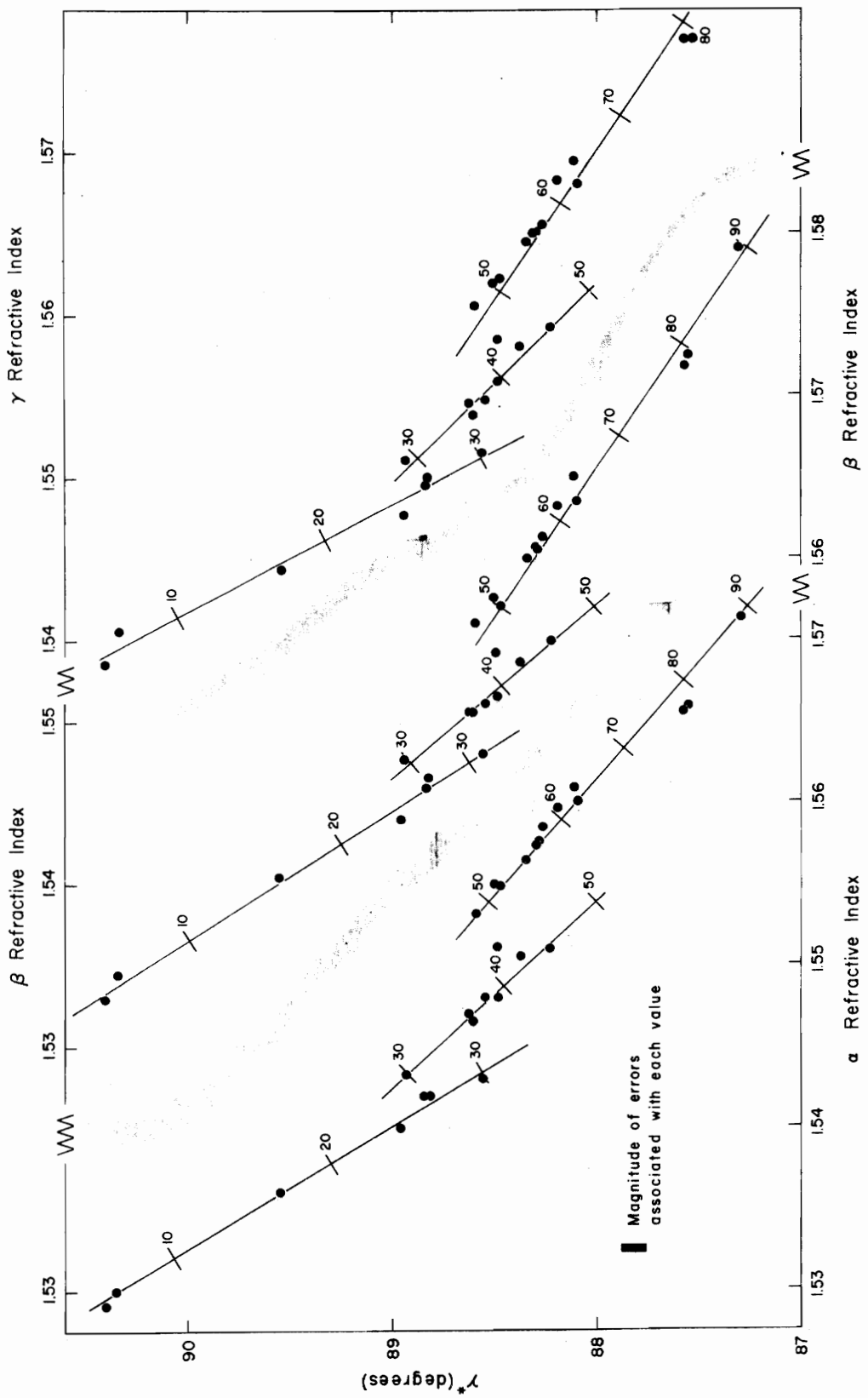

Figure 16. γ^* vs. α, β, and γ

particular curve and their correlation coefficients compared (Table 17). Thus, the correlation of each segment of the curve was slightly higher than that of the entire curve, hence yielding a basis for the supposition of discontinuities, although caution must yet be observed in that the entire range of γ^* values in which the discontinuities occur is only 0.5 degree.

Separation, δc, of e-diffractions

Gay (1956) reported continuous variation of δc with An-content whereas Doman et al. (1965) reported discontinuities in these curves. The present results (Table 18; Figure 17) can also be interpreted in terms of discontinuous curves with a break about An_{50}. The line segments on either side of the break are based only on observation because comparison of correlation coefficients for the segments and the entire curve do not yield any differences statistically, these values being:

Segment	Correlation Coefficient
1	0.898
2	0.889
Entire Curve	0.881

For any given An-content, δc obtained for this study was higher than values reported by Doman et al. (1965) but comparable to those reported by Slimming (1976), who measured the reciprocal lattice vector, S, by selected area electron diffraction (SAED) techniques, and then converted it to δc values (Figure 17).

Table 17

Correlation Coefficients for Segments of Discontinuous Curves

Segment	Correlation Coefficient	Standard Error
	An content vs. γ^*	
1	-0.996	0.07
2	-0.986	0.03
3	-0.990	0.05
Entire Curve	-0.928	0.25
	α vs. γ^*	
1	-0.997	0.06
2	-0.985	0.04
3	-0.985	0.07
Entire Curve	-0.932	0.24
	β vs. γ^*	
1	-0.996	0.07
2	-0.987	0.03
3	-0.991	0.05
Entire Curve	-0.936	0.23
	γ vs. γ^*	
1	-0.989	0.09
2	-0.978	0.04
3	-0.990	0.05
Entire Curve	-0.917	0.27

Table 18

γ^* and $\delta\underline{c}$ vs. Inferred An%

Reference #	$\alpha\beta\gamma$	Inferred An%	γ^*	$\delta\underline{c}$
99	3.6071	4.1	90.40	
110	3.6172	6.8	90.35	
129	3.6447	14.1	-----	
294	3.6541	16.6	89.55	
170	3.6798	23.5	88.94	
7106	3.6932	27.0	88.83	
31	3.6958	27.7	88.82	
33	3.7051	30.2	88.93	117.0
7123	3.7056	30.3	88.55	-----
7122a	3.7260	35.8	88.60	-----
94	3.7291	36.6	88.62	127.1
7122b	3.7328	37.6	88.54	-----
7136	3.7368	38.7	88.48	127.5
85	3.7535	43.1	88.37	148.0
7103	3.7576	44.2	88.57	137.9
22	3.7605	44.9	88.22	-----
7131	3.7719	48.0	88.59	143.2
7133	3.7825	50.8	88.50	-----
7111	3.7867	51.9	88.47	145.3
7119	3.7983	55.0	88.34	146.7
2043a	3.8039	56.5	88.29	143.0
2043b	1.8042	56.6	88.28	142.9
7100	3.8093	57.9	88.26	148.2
7101	3.8152	59.5	88.34	154.5
7113	3.8237	61.8	88.19	152.2
4087	3.8249	62.1	88.09	162.6
7115	3.8340	64.5	88.11	162.0
1090	3.8802	76.8	87.57	
1052	3.8854	78.2	87.55	
303	3.9313	90.4	87.31	

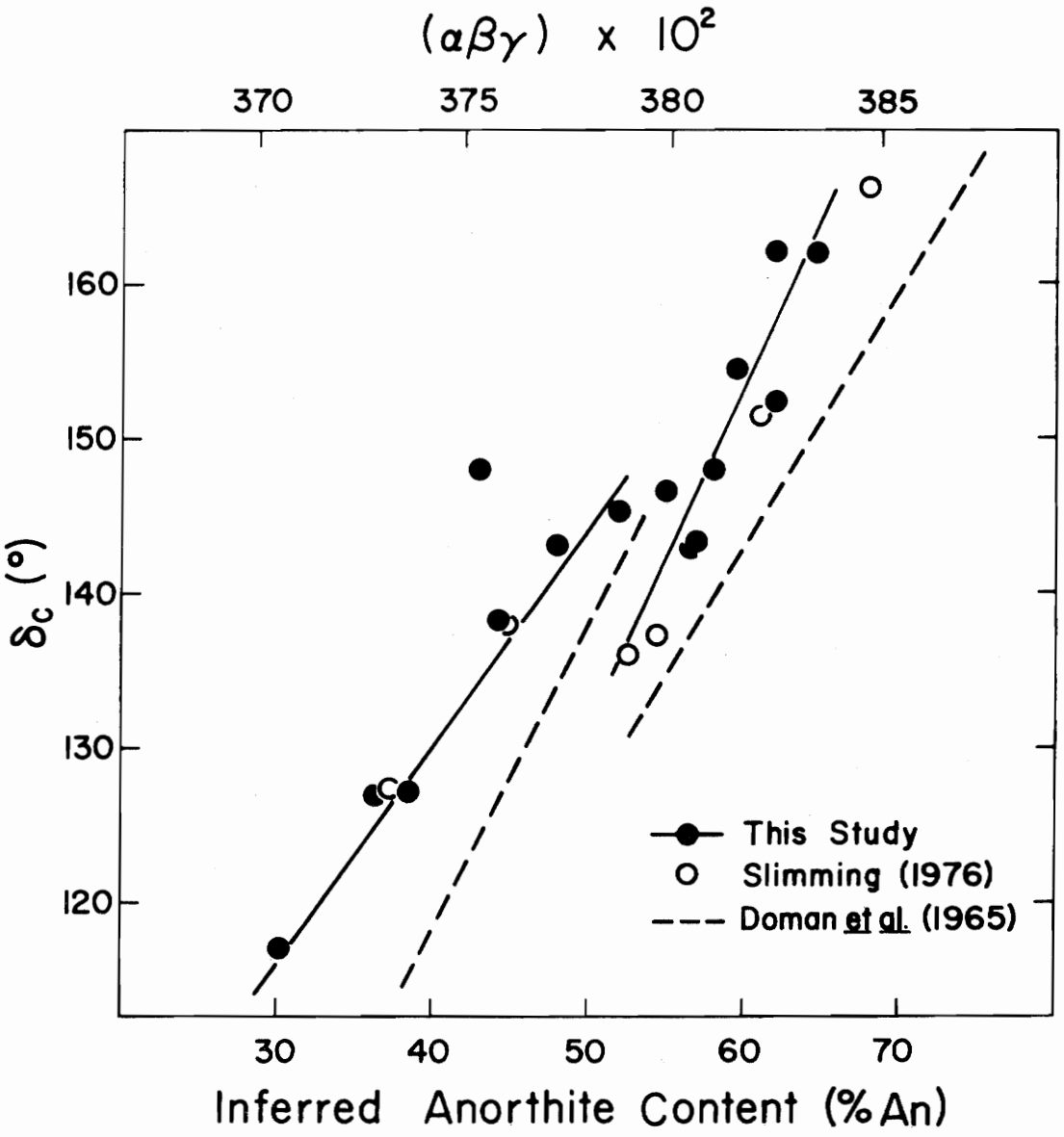

Figure 17. δc vs. inferred An-content.

Error Assessment of 2V and Co-ordinates for X, Y, and Z

For a given orientation of each grain, analysis by computer program (Bloss and Riess, 1973) of the 18 extinction readings yield a value of 2V and the S and E co-ordinates of X, Y, and Z, for which a value of the esd is computed for each. Extinction data for one orientation of Grain 7103 yielded results in part 1 of Table 19. Since it has been observed that some orientations yield better results with lower associated esd's than other orientations, the arcs of the goniometer were rotated to successive desired orientations, usually 3 per grain, and extinction values recorded and subsequently analyzed by computer. For comparison sake, the other two orientations for Grain 7103 yielded the results in parts 2 and 3 of Table 19.

In order to use this data for plotting of the migration curves, all data must be referred to the grain oriented for precession photographs, that is, (010) perpendicular to the spindle axis; hence, the sets of co-ordinates in parts 1 and 3 of Table 19 must be referred back to the orientation of the co-ordinates in part 2. This is done through the use of a program called Arcro (written by S. J. Louisnathan) (Table 19).

These values for each of the three orientations may now be averaged and their esd's calculated to yield a set of co-ordinates that have been plotted as observed values on the migration curves for each of the samples (Table 19).

Table 19

Co-ordinates of Optic Directions for Grain 7103

Results from extinction measurements

	1		2		3	
	S	E	S	E	S	E
AB	41.01(09)	36.95(06)	82.21(04)	23.71(03)	49.90(09)	45.15(03)
ON	77.41(23)	121.20(11)	63.13(42)	112.54(10)	75.96(12)	132.11(05)
OB	156.22(20)	72.24(10)	156.04(38)	96.97(12)	153.56(08)	76.63(05)
OA1	111.42(27)	36.15(16)	133.98(32)	51.67(25)	107.17(10)	46.58(07)
OA2	3.38(15)	65.55(13)	3.96(42)	39.00(27)	8.37(07)	67.13(06)
	2V = 80.34(28)		2V = 80.53(51)		2V = 80.52(12)	

Results of 1 and 3 rotated to same arc settings as 2

	1		3	
	S	E	S	E
AB	81.91	23.48	81.34	23.74
ON	64.67	112.54	64.91	112.88
OB	157.27	96.27	157.47	96.02
OA1	134.97	50.91	134.86	50.90
OA2	4.84	39.53	5.14	39.97

Results from averaging experimental 2 and rotated 1 and 3

	S	E
AB	81.82(44)	23.64(14)
ON	64.24(97)	112.65(20)
OB	156.93(77)	96.42(49)
OA1	134.60(54)	51.16(44)
OA2	4.65(54)	39.50(45)

2V = 80.46(11)

CONCLUSIONS

The present determinative curves and migration curves for the low plagioclases, except for a proposed revision of the migration curves from An_{30} to An_{55} for one optic axis, were confirmed by this study.

The structural discontinuities observed within the low plagioclase series by Doman et al. (1965) are confirmed by plots of γ^* against refractive indices, α, β, and γ, and by plots of γ^* and δc, the separation of the e-diffractions, against inferred An content. In the neighborhood of a discontinuity, two compositionally identical low plagioclases can differ in γ^* by as much as 0.4 degree. Ribbe (1972) demonstrated a direct relationship between γ^* and ΔAl, a measure of the ordering of Al into particular tetrahedral sites. Consequently, these two compositionally identical low plagioclases must differ in the degree and nature of ordering of Al within the tetrahedral sites. On the other hand, no significant changes in either refractive indices or 2V occurs across these structural discontinuities. However, on the classic migration curves, the positions of X, Y, and one optic axis are transposed for specimens $An_{30.2}$ and $An_{27.7}$. It is quite possible that the migration curves for the low plagioclases should be segmented so as to accomodate better the structural discontinuities within the series.

One important fact to remember in the preceeding conclusions is that this study also did not carry out microprobe analyses and until the K-content and trace elements are known, any relations

involving An-content are subject to change. The compositions of this study were determined by 1st degree least-squares equation which may have, in itself, destroyed any relations involving optics and An-content.

Appendix A

Migration Curves and Euler Angles

The corrected dial axis value for when the grain is oriented such that a precession photograph of the $\underline{b}^*\underline{a}^*$ reciprocal plane may be taken is plotted as a great circle with the restriction that $\underline{b}^*$ plot along the spindle axis at $\underline{S}$ = 0 degrees and $\underline{E}$ = 0 degrees (Figure 18). Perpendicular to this great circle at $\underline{E}$ = 90 degrees is, by definition, the direct crystallographic axis, $\underline{c}$. With $\underline{b}^*$ and $\underline{c}$ aligned on a great circle, the direction perpendicular to these, $\underline{A}$, is obtained by locating the point 90 degrees from this great circle (Figure 18).

For example, for Grain 7101b, the dial setting when the grain is oriented such that a precession photograph of the $\underline{b}^*\underline{a}^*$ plane may be taken is 321.6 degrees and the correction value for the goniometer head used in these determinations is 0.57 degrees, thus (321.6 + 0.57) = 322.17 degrees = 322.17 - 180 = 142.17 degrees, the corrected dial axis reading, $\underline{D}$, to be used when plotting the plane stereographically. Consequently, the $\underline{a}^*\underline{b}^*$ plane coincides with the great circle at $\underline{S}$ = 142.17 degrees (Figure 18). Direct axis $\underline{c}$, the pole to this plane, thus has co-ordinates $\underline{S}$ = 142.17 - 90 = 52.17 degrees and $\underline{E}$ = 90 degrees. The third direction, $\underline{A}$, has $\underline{S}$ = 142.17 degrees and $\underline{E}$ = 90 degrees. Although both are plotted at the same position, the two points do not coincide, with $\underline{A} \wedge \underline{a}^*$ being 1.76 degrees.

The extinction program supplies the $\underline{S}$ and $\underline{E}$ co-ordinates of the

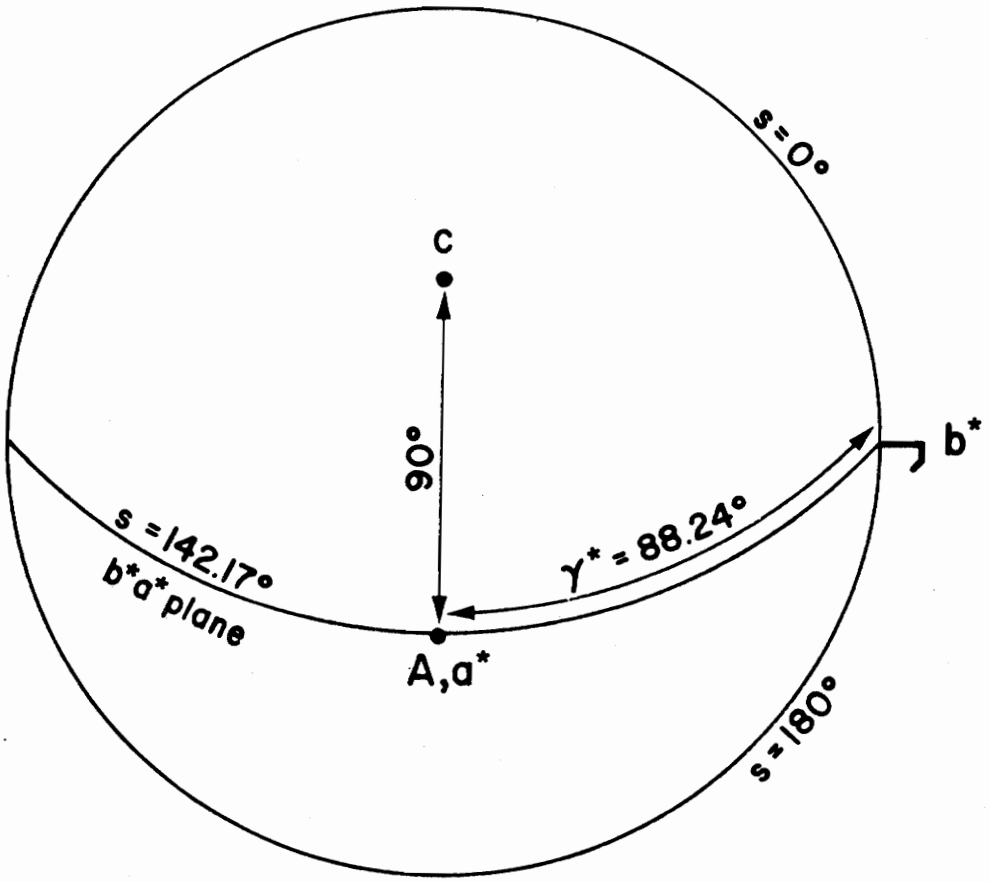

Figure 18. Stereographic projection to depict plotting of the crystallographic related directions and optic directions.

optic axes and principal vibration directions, and for Grain 7101b:

	OA1	OA2	OB(X)	ON(Y)	AB(Z)
S	159.67	39.64	17.71	115.42	76.62
E	32.15	61.36	106.60	114.21	29.99

In order to compare my migration curves with those of Burri et al. (1967), a standard orientation of the crystallographic directions was adopted such that b* plots along the spindle axis, A plots at S = 180 degrees and E = 90 degrees, and c is perpendicular to the plane of the stereonet at S = 90 degrees and E = 90 degrees. All directions must be rotated along small circles of the stereonet (Figure 19) until the required orientation is achieved. In this case, a rotation of 37.83 degrees is needed, hence the new co-ordinates are:

	OA1	OA2	OB(X)	ON(Y)	AB(Z)
S	17.50	77.47	55.54	153.25	114.45
E	147.85	61.36	106.60	114.21	29.99

In order to calculate Euler angles, we need the co-ordinates of the line of intersection between the two planes whose poles are the c crystallographic axis and X, this line of intersection being called the nodal line, NL (Figure 20). The positive end of the nodal line is labelled +NL, hence the S co-ordinate = 180 degrees. The E value of the nodal line may be calculated from the equation; (Bloss, The Spindle Stage, in press)

$$\tan E_{NL} = \frac{-1}{\tan E_{OB} \cos (S_{OB} - S_{NL})}$$

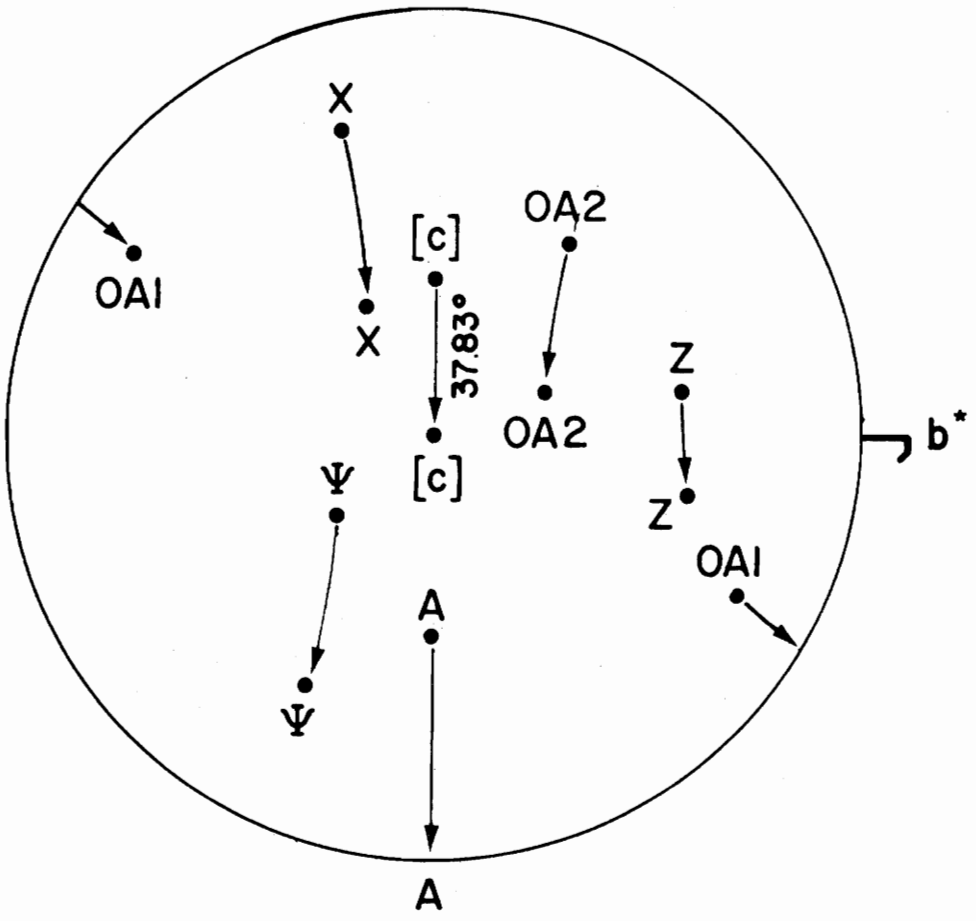

Figure 19. Stereographic projection to depict the rotation of crystallographic related directions and optic directions about small circles of the stereonet to achieve a standard orientation of the crystallographic related directions.

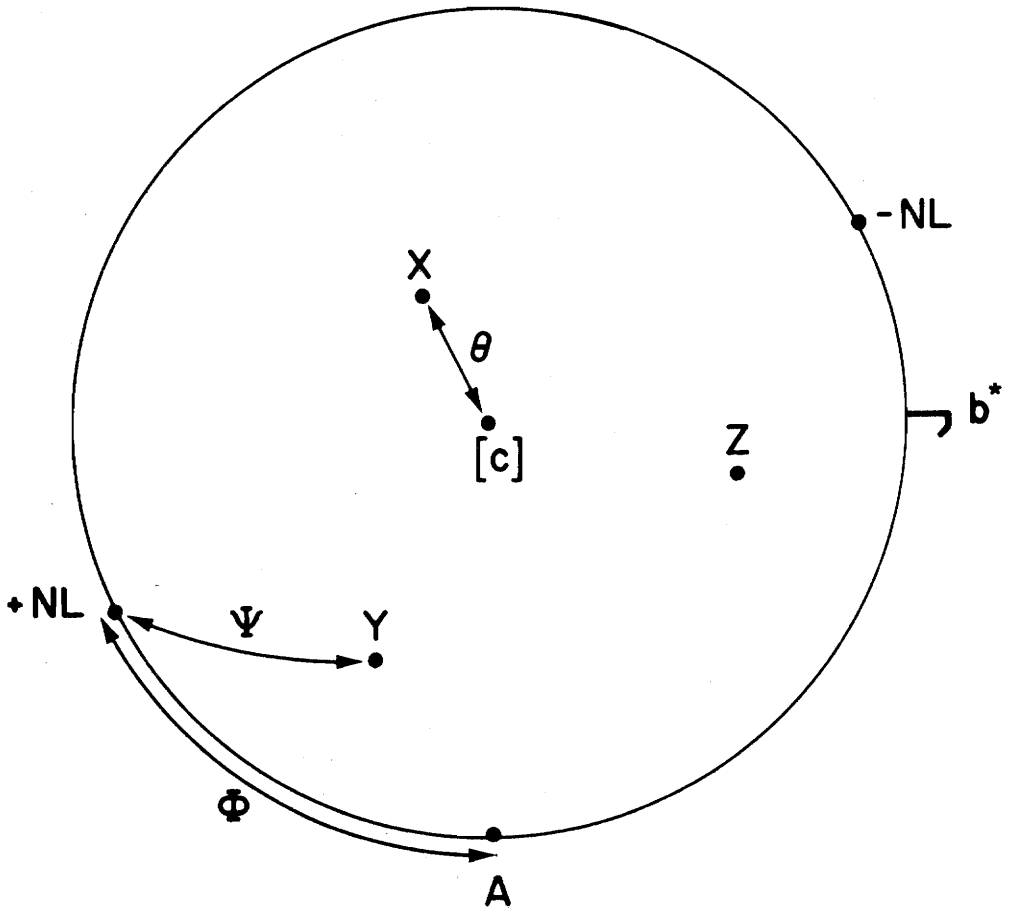

Figure 20. Stereographic projection to depict Euler angles Φ, Θ, and Ψ.

$$\tan E_{\underline{NL}} = \frac{-1}{\tan 106.60 \cos (55.54 - 180)}$$

$$E_{\underline{NL}} = 152.22 \text{ degrees} \quad .$$

All the co-ordinates needed to calculate Euler angles Φ, Θ, and Ψ are now known. First, Φ is defined as a right handed rotation about the $+\underline{c}$ crystallographic axis such that $+\underline{A}$ is brought into coincidence with the nodal line, $+\underline{NL}$ (Figures 7 and 20). This value is equal to $+\underline{c} \wedge +\underline{NL}$ and is merely $E_{\underline{NL}} - E_{\underline{A}} = 152.22 - 90 = 62.22$ degrees.

The second Euler angle, Θ, (Figures 7 and 20) is defined as a rotation about the nodal line such that $+\underline{c}$ is made coincident with $+\underline{X}$, thus equal to $+\underline{c} \wedge +\underline{X}$. This angle may be calculated from:

$$\cos \Theta = \sin E_{\underline{X}} \cos(S_{\underline{X}} - S_{\underline{c}})$$

$$\cos \Theta = \sin 106.60 \cos (55.54 - 90)$$

$$\Theta = 37.80 \text{ degrees} \quad .$$

The last Euler angle, Ψ, (Figures 7 and 20) is defined as a right handed rotation about $+\underline{X}$ such that $+\underline{A}$ is made coincident with $+\underline{Y}$, as calculated from:

$$\cos \Psi = \cos E_{\underline{Y}} \cos E_{\underline{A}} + \sin E_{\underline{Y}} \sin E_{\underline{A}} \cos (S_{\underline{Y}} - S_{\underline{A}})$$

$$\cos \Psi = \cos 114.21 \cos 152.22 + \sin 114.21 \sin 152.22 \cos (153.25 - 180)$$

$$\Psi = 42.06 \text{ degrees.}$$

BIBLIOGRAPHY

Allen, R. D. (1956) A new equation relating index of refraction and specific gravity. *Amer. Mineral.* 41, 245-267.

Balconi, M., Zezza, U. (1968) Considerazioni sulla determinazione per via ottica dello stato termico dei plagioclasi curve % An 2V. *Periodico di Mineralogia* 37, 67-127.

Bambauer, H. U., Corlett, M., Eberhard, E., Viswanthan, K. (1967) Diagrams for the determination of plagioclases using x-ray methods. (Part III of labratory investigations on plagioclases). *Schweiz. Mineral. Petrogr. Mitt.* 47, 333-350.

Barth, T. F. W. (1931) Permanent changes in the optical orientation of feldspars exposed to heat. *Norsk Geologiok Tidsskrift* 12, 57-72.

Bloss, F. D. (1962) Relationship between density and composition in mol per cent for some solid solution series. *Amer. Mineral.* 37, 966-981.

Bloss, F. D. (in press) *The Spindle Stage*. Geopress, P. O. Box 2604, Cambria Station, Virginia 24073

Bloss, F. D., Riess, D. (1973) Computer determination of 2V and indicatrix orientation from extinction data. *Amer. Mineral.* 58, 1052-1061.

Bown, M. G., Gay, P. (1969) The effect of heat treatment on the diffraction patterns of intermediate plagioclase. *Z. Kristallogr.* 129, 451-457.

Burri, C., Parker, R. L., Wenk, E. (1962) The optical orientation

of the plagioclases. *Norsk Geologiok Tidsskrift* 42, 207-214.

Burri, C., Parker, R. L., Wenk, E. (1967) *Die optische Orientierung der Plagioklase-unterlagen und Diagramme zur Plagioklasbestimmung nach der drehtische Methode*. 334 pp. Basel and Stuttgart: Birkhauser.

Chao, S. H., Taylor, W. H. (1940) Isomorphous replacement and superlattice structures in the plagioclase feldspars. *Proc. Roy. Soc. London*, 176A, 76-87.

Chayes, F. (1950) On the relation between anorthite content and γ-index of natural plagioclases. *Amer. Jour. Sci.* 58, 593-595.

Chayes, F. (1952) Relations between composition and indices of refraction in natural plagioclases. *Amer. Jour. Sci., Bowen Vol.*, 85-105.

Chayes, F. (1954) A test of the revised determinative chart for plagioclases. *Amer. Jour. Sci.* 252, 172-180.

Cole, W. F., Sorum, H., Taylor, W. H. (1951) The structure of the plagioclase felspars I. *Acta. Crystallogr.* 4, 20-29.

Corlett, M., Eberhard, E. (1967) Das material fur chemische und physikalische untersuchungen an plagioklasen. (Teil I der laboratoriumsuntersuchungen an plagioklasen). *Schweiz. Mineral. Petrogr. Mitt.* 47, 303-316.

Dana, E. D. (1920) *The system of mineralogy of James Dwight Dana 1837-1868. Descriptive Mineralogy*. Sixth Edition, New York: John Wiley and Sons.

Deer, W. A., Howie, R. A., Zussman, J. (1963) *Rock Forming Minerals*,

4, Framework Silicates. 435 pp. London: Longmans, Green and Company, Ltd.

Doman, R. C., Cinnamon, C. G., Bailey, S. W. (1965) Structural discontinuities in the plagioclase feldspar series. *Amer. Mineral.* 50, 724-740.

Emmons, R. C., (Ed.), Gates, R. M., Clabaugh, S. E., Crump, R. M., Ketner, K. B., Mann, V., Reynolds, C. D., Saunders, D. F., Bradley, C., Lyons, E. J. (1953) Selected petrogenetic relationships of plagioclase. *Geol. Soc. Amer., Memoir 52,* 142 pp.

Federow, E. (1893) Universal methode in der mineralogie und petrographie. I. Teil universalgeometrische untersuchungen. *Z . Kristallogr.* 21, 574-714.

Foit, F. F., Peacor, D. R. (1967) High temperature diffraction data on selected reflections of an andesine and anorthite. *Z. Kristallogr.* 125, 1-6.

Gay, P. (1956) The structure of the plagioclase feldspars: VI. Natural intermediate plagioclases. *Mineral Mag.* 31, 21-40.

Gay, P., Bown, M. G. (1956) The structures of the plagioclase feldspars. VII. The heat treatment of intermediate plagioclases. *Mineral Mag.* 31, 306-313.

Gay, P., Muir, I. D. (1962) Investigation of the feldspars of the Skaergaard Intrusion, Eastern Greenland. *Jour. Geol.* 70, 565-581.

Kitamura, M., Morimoto, N. (1975) The superstructure of intermediate plagioclase. *Proc. Japan Acad.* 51, 419-424.

Kohler, A. (1942a) Die abhangigkeit der plagioklasoptik vom vorange-

gangenen warmeverhalten. *Tschermaks Mineral. und Petrogr. Mitt.* 53, 24-49.

Kohler, A. (1942b) Drehtischmessungen an plagioklaszwillingen von tief- und hochtemperaturoptik. *Tschermaks Mineral. und Petrogr. Mitt.* 53, 159-179.

Larsson, W. (1941) Petrology of interglacial volcanics from the Andes of northern Patagonia. *Bull. Geol. Inst. Univ. (Upsala)* 28, 191-405.

Marfunin, A. S. (1966) *The Feldspars: Phase Relations, Optical Properties, and Geological Distribution.* (Trans from the Russian edition, 1962). Jerusalem (Israel Prog. Sci. Translations), 317 pp.

Megaw, H. D. (1960) Order and disorder. I. Theory of stacking faults and diffraction maxima. II. Theory of diffraction effects in the intermediate plagioclase feldspars. III. The structure of the intermediate plagioclase feldspars. *Proc. Roy. Soc.* 259A, 59-78, 159-183, 184-202.

Morimoto, N., Nakajima, Y., Kitamura, M. (1975a) Direct observation of the superstructure of labradorite by electron microscopy. *Proc. Japan Acad.* 51, 725-728.

Morimoto, N., Kitamura, M., Nakajima, Y. (1975b) Antiphase relations in superstructures of the e-plagioclase. *Proc. Japan Acad.* 51, 729-732.

Plas, L. van der (1966) *The Identification of Detrital Feldspars.* Amsterdam: Elsevier 305 pp.

Reinhart, M. (1931) *Universal Drehtischmethoden.* Basel: Wepf et Cie,

OPTICAL AND X-RAY STUDY OF THE LOW PLAGIOCLASES

by

Hugh Edward Wolfe

(ABSTRACT)

For each of 24 grains of low plagioclase with 'Inferred An' contents 4.1, 6.8, 16.6, 27.7, 30.2, 35.8, 36.6, 37.6, 38.7, 43.1, 44.2, 48.0, 50.8, 51.9, 55.0, 56.5, 56.6, 57.9, 61.8, 62.1, 64.5, 76.8, 78.2, and 90.4 the following properties were measured: (1) γ^*, (2) location of the crystallographic axes, (3) separation of the non-Bragg e-diffractions from precession photographs, (4) refractive indices α, β, and γ, (5) the location of the optic axes, (6) the location of the principal vibration directions $\underline{X}$, $\underline{Y}$, and $\underline{Z}$, (7) and a value of 2V.

Plots of γ^* versus the product, $\alpha\beta\gamma$, which correlates linearly to anorthite content, confirm the presence of two structural discontinuities in the low plagioclase series. The angular attitude of the two optic axes and of the principal vibration directions plotted stereographically relative to $\underline{b}^*$ (at $\underline{S} = 0$, $\underline{E} = 0$) and $\underline{c}$ (at $\underline{S} = 90$, $\underline{E} = 90$) for each grain follow the classic migration curves of Reinhart (1931) with slight revision. The orientation of the principal vibration axes $\underline{X}$, $\underline{Y}$, and $\underline{Z}$ is related quantitatively to crystallographic directions $\underline{b}^*$, $\underline{c}$, and $\underline{A}$ by means of Euler angles Φ, Θ, and Ψ introduced by Burri *et al.* (1967) and to the crystallographic axes $\underline{a}$, $\underline{b}^*$, and $\underline{C}$ by a set of new Euler angles θ_1, θ_2, and θ_3.